

---

# EFFICIENT ADVERSARIAL CONTRASTIVE LEARNING VIA ROBUSTNESS-AWARE CORESET SELECTION

---

Xilie Xu<sup>1\*</sup>, Jingfeng Zhang<sup>2\*</sup>, Feng Liu<sup>3</sup>, Masashi Sugiyama<sup>2,4</sup>, Mohan Kankanhalli<sup>1</sup>

<sup>1</sup> School of Computing, National University of Singapore

<sup>2</sup> RIKEN Center for Advanced Intelligence Project (AIP)

<sup>3</sup> School of Mathematics and Statistics, The University of Melbourne

<sup>4</sup> Graduate School of Frontier Sciences, The University of Tokyo

## ABSTRACT

Adversarial contrastive learning (ACL) does not require expensive data annotations but outputs a robust representation that withstands adversarial attacks and also generalizes to a wide range of downstream tasks. However, ACL needs tremendous running time to generate the adversarial variants of all training data, which limits its scalability to large datasets. To speed up ACL, this paper proposes a *robustness-aware coreset selection* (RCS) method. RCS does not require label information and searches for an informative subset that minimizes a representational divergence, which is the distance of the representation between natural data and their virtual adversarial variants. The vanilla solution of RCS via traversing all possible subsets is computationally prohibitive. Therefore, we theoretically transform RCS into a surrogate problem of submodular maximization, of which the greedy search is an efficient solution with an optimality guarantee for the original problem. Empirically, our comprehensive results corroborate that RCS can speed up ACL by a large margin without significantly hurting the *robustness and standard transferability*. Notably, to the best of our knowledge, we are the first to conduct ACL efficiently on the large-scale ImageNet-1K dataset to obtain an effective robust representation via RCS.

## 1 Introduction

The pre-trained models can be easily finetuned to downstream applications, recently attracting increasing attention (Deng et al., 2009; Ridnik et al., 2021). Notably, vision Transformer (Dosovitskiy et al., 2020) pre-trained on ImageNet-1K (Deng et al., 2009) can achieve state-of-the-art performance on many downstream computer-vision applications (Krizhevsky, 2009; Zhai et al., 2019). Foundation models (Bommasani et al., 2021) trained on large-scale unlabeled data (such as GPT (Brown et al., 2020) and CLAP (Elizalde et al., 2022)) can be adapted to a wide range of downstream tasks. Due to the prohibitively high cost of annotating large-scale data, the pre-trained models are commonly powered by the techniques of unsupervised learning (Chen and He, 2021; Le-Khac et al., 2020) in which *contrastive learning* (CL) is the most effective learning style to obtain the generalizable feature representations (Chen et al., 2020; Jiang et al., 2020).

*Adversarial CL* (ACL) (Jiang et al., 2020) yields a robust representation that is both adversarially robust and generalizable. Compared with the standard CL (Chen et al., 2020), ACL can output a robust representation that can transfer some robustness to the downstream tasks against adversarial attacks via robust finetuning (Jiang et al., 2020; Fan et al., 2021). Besides, as shown in Figure 1, the downstream tasks standardly finetuned from a robust representation have even better standard accuracies than those from the standard CL, which resonates with the recent findings that adversarially robust models benefit standard accuracy on downstream classification tasks (Salman et al., 2020; Xu et al., 2022).

However, ACL is computationally expensive, which limits its scalability. At each training epoch, ACL first needs to conduct several backward propagations (BPs) on all training data to generate their adversarial variants and then train the model with those adversarial data. Even if we use the techniques of fast adversarial training (Wong et al., 2020;

---

\*Equal contributions.

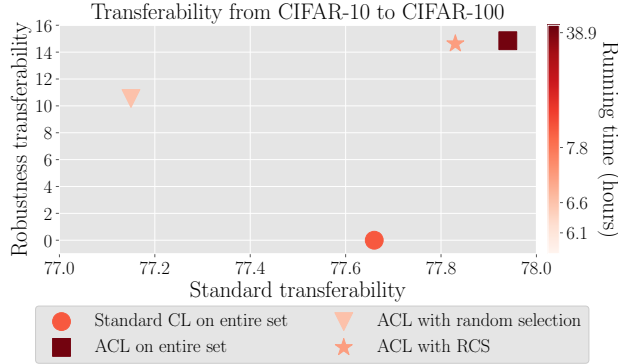


Figure 1: We learn a representation based on CIFAR-10 dataset (without requiring labels) using both standard CL and ACL manner, then we evaluate the representation’s robustness/standard transferability to CIFAR-100 dataset (using labels during fine-tuning). We demonstrate the running time of obtaining a representation by standard CL and ACL w.r.t. different coreset selection (CS) strategies, and robustness/standard transferability that is measured by robust/standard test accuracy on CIFAR-100 after robust/standard finetuning. Experimental details are in Appendix B.3.

Shafahi et al., 2019) that significantly reduce the need for conducting BPs per data, ACL still encounters the issue of the large scale of the training set that is commonly used for pre-training a useful representation.

*Coreset selection* (CS) (Feldman, 2020) that selects a small yet informative subset can reduce the need for the whole training set, but CS cannot be applied to ACL directly. Mirzasoleiman et al. (2020) and Killamsetty et al. (2021a;b;c) have significantly accelerated the standard training by selecting an informative training subset. Recently, Dolatabadi et al. (2022) proposed an adversarial CS method to accelerate the standard adversarial training (Madry et al., 2018; Zhang et al., 2019) by selecting a representative subset that can accurately align the gradient of the full set. However, the existing CS methods require the label information of training data, which are not applicable to the ACL that learns from the unlabeled data.

To accelerate the ACL, this paper proposes a robustness-aware coreset selection (RCS) that selects a coreset without requiring the label information but still helps ACL to obtain an effective robust representation. RCS searches for a coreset that minimizes the representational divergence (RD) of a representation. RD measures the representation difference between the natural data and their virtual adversarial counterparts (Miyato et al., 2018), in which virtual adversarial data can greatly alter the output distribution in the sense of feature representation.

Although solving the RCS via traversing all possible subsets is simple, it is computationally prohibitive. Therefore, we transform the RCS into a proxy problem of maximizing a set function that is theoretically shown monotone and  $\gamma$ -weakly submodular (see Theorem 1) subject to cardinality constraints (Das and Kempe, 2011; Gatmiry and Gomez-Rodriguez, 2021). Then, we can apply the greedy search (Das and Kempe, 2011) to efficiently find a coreset that can minimize the RD. Notably, Theorem 2 provides the theoretical guarantee of optimality of our greedy-search solution.

Empirically, we demonstrate RCS can indeed speed up ACL (Jiang et al., 2020). As shown in Figure 1, RCS can speed up ACL by 6 times and obtain an effective representation without significantly hurting the *robustness and standard transferability* (details in Section 4.1). Notably, to the best of our knowledge, we are the first to apply ACL on the large-scale ImageNet-1K (Deng et al., 2009) dataset to obtain a robust representation via RCS (see Section 4.3). Besides, we empirically show that RCS is compatible with standard adversarial training (Madry et al., 2018; Zhang et al., 2019) as well in Section 4.2. Our comprehensive experiments corroborate that our proposed RCS is a unified and principled framework for efficient robust learning.

## 2 Background and Preliminaries

In this section, we introduce related works and preliminaries about contrastive learning.

### 2.1 Related Works

**Contrastive learning (CL).** CL approaches are frequently used to leverage large unlabeled datasets for learning useful representations. Previous unsupervised methods that map similar samples to similar representations (Koch et al., 2015) have the issue of collapsing to a constant representation. CL addresses the representational collapse by introducing the negative samples (Le-Khac et al., 2020). Chen et al. (2020) presented SimCLR that leverages

the contrastive loss for learning useful representations and achieved significantly improved accuracy on the standard suit of downstream tasks. Recently, adversarial contrastive learning (ACL) (Kim et al., 2020; Jiang et al., 2020; Ho and Nvasconcelos, 2020; Fan et al., 2021; Yu et al., 2022; Zhang et al., 2022a) that incorporates adversarial training with the contrastive loss (Chen et al., 2020) has become the most effective unsupervised approaches to learn robust representations. Jiang et al. (2020) showed that ACL could exhibit better adversarial robustness on downstream tasks compared with standard CL (i.e., SimCLR (Chen et al., 2020)). Fan et al. (2021) further demonstrated that ACL can lead to a more clear decision boundary, thus enhancing the robustness transferability.

Unexpectedly, ACL needs large computational resources to obtain useful representations from large-scale datasets. ACL needs to spend a large amount of running time generating adversarial training data during pre-training. Fast adversarial training (AT) (Wong et al., 2020) uses the fast gradient descent method (FGSM) (Goodfellow et al., 2014) to accelerate the generation procedure of adversarial training data, thus speeding up robust training. A series of recent works (Andriushchenko and Flammarion, 2020; Zhang et al., 2022b) followed this line and further improved the performance of fast AT. However, the time complexity of ACL is still proportional to the size of the training set. Besides, the large-scale training sets (e.g., ImageNet-1K (Deng et al., 2009) contains over 1 million training images) further contribute to the inefficiency of adversarially pre-training procedures (Salman et al., 2020; Xu et al., 2022). To enable efficient ACL, we propose a novel CS method that can speed up ACL by decreasing the amount of training data.

**Coreset selection (CS).** CS aims to select a small yet informative data subset that can approximate certain desirable characteristics (e.g., the loss gradient) of the entire set (Feldman, 2020). Several studies have shown that CS is effective for efficient standard training in supervised (Mirzasoleiman et al., 2020; Killamsetty et al., 2021b;a) and semi-supervised (Killamsetty et al., 2021c) settings. Dolatabadi et al. (2022) proposed adversarial coreset selection (ACS) that selects representative coresets of adversarial training data that can estimate the adversarial loss gradient on the entire training set. However, ACS is only adapted to supervised AT (Madry et al., 2018; Zhang et al., 2019). Thus, ACS requires the label information and is not applicable to ACL. In addition, previous studies did not explore the influence of CS on the pre-trained model’s transferability. To this end, we propose a novel CS method that does not require label information, and empirically demonstrate that our proposed method can significantly accelerate ACL while only slightly hurting the transferability of pre-trained models.

## 2.2 Preliminaries

Here, we introduce the preliminaries of adversarial contrastive learning (ACL) (Jiang et al., 2020) and finetuning procedure.

Let  $(\mathcal{X}, d_\infty)$  be the input space  $\mathcal{X}$  with the infinity distance metric  $d_\infty(x, x') = \|x - x'\|_\infty$ , and

$$\mathcal{B}_\epsilon[x] = \{x' \in \mathcal{X} \mid d_\infty(x, x') \leq \epsilon\} \quad (1)$$

be the closed ball of radius  $\epsilon > 0$  centered at  $x \in \mathcal{X}$ .

**ACL (Jiang et al., 2020).** Prior to ACL, we first introduce the standard contrastive loss (Chen et al., 2020). Let  $f_\theta : \mathcal{X} \rightarrow \mathcal{Z}$  be a feature extractor parameterized by  $\theta$ ,  $g : \mathcal{Z} \rightarrow \mathcal{V}$  be a projection head that maps representations to the space where the contrastive loss is applied, and  $\tau_i, \tau_j : \mathcal{X} \rightarrow \mathcal{X}$  be two transformation operations randomly sampled from a pre-defined transformation set  $\mathcal{T}$ . Given a minibatch  $B \sim \mathcal{X}^\beta$  consisting of  $\beta$  samples, we denote the augmented minibatch  $B' = \{\tau_i(x_k), \tau_j(x_k) \mid \forall x_k \in B\}$  consisting of  $2\beta$  samples. We take  $h_\theta(\cdot) = g \circ f_\theta(\cdot)$  and  $x_k^u = \tau_u(x_k)$  for any  $x_k \sim \mathcal{X}$  and  $u \in \{i, j\}$ . The standard contrastive loss of a positive pair  $(x_k^i, x_k^j)$  is as follows:

$$\ell_{\text{CL}}(x_k^i, x_k^j; \theta) = - \sum_{u \in \{i, j\}} \log \frac{e^{\text{sim}(h_\theta(x_k^i), h_\theta(x_k^j))/t}}{\sum_{x \in B' \setminus \{x_k^u\}} e^{\text{sim}(h_\theta(x_k^u), h_\theta(x))/t}},$$

where  $\text{sim}(p, q) = p^\top q / \|p\| \|q\|$  is the cosine similarity function and  $t > 0$  is a temperature parameter.

Given an unlabeled set  $X \sim \mathcal{X}^N$  consisting of  $N$  samples, the loss function of ACL (Jiang et al., 2020) is  $\mathcal{L}_{\text{ACL}}(X; \theta) = \sum_{k=1}^N \ell_{\text{ACL}}(x_k; \theta)$  where

$$\ell_{\text{ACL}}(x_k; \theta) = \max_{\substack{\tilde{x}_k^i \in \mathcal{B}_\epsilon[x_k^i] \\ \tilde{x}_k^j \in \mathcal{B}_\epsilon[x_k^j]}} \ell_{\text{CL}}(\tilde{x}_k^i, \tilde{x}_k^j; \theta) + \ell_{\text{CL}}(x_k^i, x_k^j; \theta),$$

in which  $\tilde{x}_k^i$  and  $\tilde{x}_k^j$  are adversarial data generated via projected gradient descent (PGD) (Madry et al., 2018) within the  $\epsilon$ -balls centered at  $x_k^i$  and  $x_k^j$ . Given an initial positive pair  $(x^{i,(0)}, x^{j,(0)})$ , PGD step  $T \in \mathbb{N}$ , step size  $\rho > 0$ , and adversarial budget  $\epsilon \geq 0$ , PGD iteratively updates the pair of data from  $\tau = 0$  to  $T - 1$  as follows:

$$\begin{aligned} x^{i,(\tau+1)} &= \Pi_{\mathcal{B}_\epsilon[x^i,(0)]}(x^{i,(\tau)} + \rho \text{sign}(\nabla_{x^i,(\tau)} \ell_{\text{CL}}(x^{i,(\tau)}, x^{j,(\tau)})), \\ x^{j,(\tau+1)} &= \Pi_{\mathcal{B}_\epsilon[x^j,(0)]}(x^{j,(\tau)} + \rho \text{sign}(\nabla_{x^j,(\tau)} \ell_{\text{CL}}(x^{i,(\tau)}, x^{j,(\tau)})), \end{aligned}$$

where  $\Pi_{\mathcal{B}_\epsilon[x]}$  projects the data into the  $\epsilon$ -ball around the initial point  $x$ .

ACL is realized by conducting one step of inner maximization on generating adversarial data via PGD and one step of outer minimization on updating  $\theta$  by minimizing the ACL loss on generated adversarial data, alternatively. Note that the parameters of the projection head  $g$  are updated as well during ACL. Here we omit the parameters of  $g$  for notational simplicity since we only use the parameters of feature extractor  $f_\theta$  on downstream tasks after completing ACL. When ACL’s adversarial budget  $\epsilon$  is set to 0, it is exactly standard CL; otherwise, when  $\epsilon > 0$ , it is ACL.

**Robust finetuning.** We leverage standard adversarial training (SAT) (Madry et al., 2018) for robust finetuning on downstream tasks, similar to Hendrycks et al. (2019). Given a labeled dataset  $D = \{(x_i, y_i)\}_{i=1}^{N'}$  consisting of  $N'$  samples, where data point  $x_i \in \mathcal{X}$  and label  $y_i \in \mathcal{Y} = \{0, 1, \dots, C - 1\}$ , a pre-trained feature extractor  $f_\theta : \mathcal{X} \rightarrow \mathcal{Z}$ , and a randomly initialized classifier  $\phi_{\theta_c} : \mathcal{Z} \rightarrow \mathbb{R}^C$ , the loss function of robust finetuning is

$$\mathcal{L}_{\text{Robust}}(D; \{\theta, \theta_c\}) = \sum_{i=1}^{N'} \max_{\tilde{x}_i \in \mathcal{B}_\epsilon[x_i]} \ell(\phi_{\theta_c} \circ f_\theta(\tilde{x}_i), y_i),$$

where  $\ell(\cdot, \cdot)$  is the cross-entropy (CE) loss and  $\tilde{x}_i$  is adversarial training data generated by PGD within the  $\epsilon$ -ball centered at  $x_i$ .

**Standard finetuning.** Following Salman et al. (2020), we use standard training whose loss function is shown below for standard finetuning:

$$\mathcal{L}_{\text{Standard}}(D; \{\theta, \theta_c\}) = \sum_{i=1}^{N'} \ell(\phi_{\theta_c} \circ f_\theta(x_i), y_i),$$

where  $\ell(\cdot, \cdot)$  is the CE loss. According to the range of parameters that are allowed to be updated during finetuning, finetuning is divided into the following two situations: (a) full finetuning that finetunes all the parameters,

$$\textbf{Full finetuning: } \{\theta^*, \theta_c^*\} = \arg \min_{\{\theta, \theta_c\}} \mathcal{L}(D; \{\theta, \theta_c\}),$$

and (b) partial finetuning that only finetunes the classifier’s parameters,

$$\textbf{Partial finetuning: } \theta_c^* = \arg \min_{\theta_c} \mathcal{L}(D; \{\theta, \theta_c\}),$$

where  $\mathcal{L}(\cdot)$  can be replaced by  $\mathcal{L}_{\text{Robust}}(\cdot)$  and  $\mathcal{L}_{\text{Standard}}(\cdot)$ . Therefore, there are four types of finetuning methods used in our paper, i.e., robust/standard full/partial finetuning. Note that the *robustness/standard transferability* refers to the robust/standard test accuracy on the downstream task of the pre-trained model after robust/standard finetuning.

### 3 Robustness-Aware Coreset Selection

In this section, we first introduce the representational divergence (RD), which is quantified by the distance of the representation between natural data and their virtual adversarial variants, as the measurement of the adversarial robustness of a representation. Then, we formulate the learning objective of the Robustness-aware Coreset Selection (RCS). Next, we theoretically show that our proposed RCS can be efficiently solved via greedy search. Finally, we give the algorithm of efficient ACL via RCS.

#### 3.1 Representational Divergence (RD)

Adversarial robustness is the most significant property of adversarially pre-trained models, which could lead to enhanced robustness and standard transferability. Inspired by previous studies (Zhang et al., 2019; Zhang and Wang, 2019), we measure the adversarial robustness of the representation in an unsupervised manner using the representational

divergence (RD). Given a natural data point  $x \sim \mathcal{X}$  and a model  $g \circ f_\theta : \mathcal{X} \rightarrow \mathcal{V}$  composed of a feature extractor  $f_\theta$  and a projector head  $g$ , RD of this data point  $\ell_{\text{RD}}(x; \theta)$  is quantified by the distance between the representation of the natural data and that of its virtual adversarial counterpart (Miyato et al., 2018), i.e.,

$$\ell_{\text{RD}}(x; \theta) = d(g \circ f_\theta(\tilde{x}), g \circ f_\theta(x)) \quad \text{s.t.} \quad \tilde{x} = \arg \max_{x' \in \mathcal{B}_\epsilon[x]} d(g \circ f_\theta(x'), g \circ f_\theta(x)), \quad (2)$$

in which  $\tilde{x}$  is the adversarial data generated via PGD within the  $\epsilon$ -ball centered at  $x$  and  $d(\cdot, \cdot) : \mathcal{V} \times \mathcal{V} \rightarrow \mathbb{R}$  is a distance function, such as the Kullback–Leibler (KL) divergence (Zhang et al., 2019), the Jensen-Shannon (JS) divergence (Addepalli et al., 2022), and the optimal transport (OT) distance (Zhang and Wang, 2019). We denote the RD on the unlabeled set  $X$  as  $\mathcal{L}_{\text{RD}}(X; \theta) = \sum_{x_i \in X} \ell_{\text{RD}}(x_i; \theta)$ . The smaller the RD is, the representations are of less sensitivity to adversarial perturbations, thus being more robust.

### 3.2 Learning Objective of Robustness-Aware Coreset Selection (RCS)

Our proposed RCS aims to select an informative subset that can achieve the minimized RD between natural data and their adversarial counterparts, thus expecting the selected coreset to be helpful to improve the adversarial robustness of representations. Therefore, given an unlabeled training set  $X \sim \mathcal{X}^N$  and an unlabeled validation set  $U \sim \mathcal{X}^M$  composed of  $N$  and  $M$  ( $M \ll N$ ) samples respectively, our proposed Robustness-aware Coreset Selection (RCS) searches for a coreset  $S^*$  such that

$$S^* = \arg \min_{S \subseteq X, |S|/|X| \leq k} \mathcal{L}_{\text{RD}}(U; \arg \min_{\theta} \mathcal{L}_{\text{ACL}}(S; \theta)). \quad (3)$$

Note that the subset fraction  $k \in (0, 1]$  controls the size of the coreset, i.e.,  $|S^*| \leq kN$ . RCS only needs to calculate RD on the validation set (i.e.,  $\mathcal{L}_{\text{RD}}(U)$ ) and ACL loss on the subset (i.e.,  $\mathcal{L}_{\text{ACL}}(S)$ ), which can be computed in an unsupervised manner. Thus, RCS is applicable to ACL on unlabeled datasets, and compatible with supervised AT on labeled datasets as well, such as SAT (Madry et al., 2018) and TRADES (Zhang et al., 2019) (details in Appendix B.9). Intuitively, the coreset  $S^*$  found by RCS can make the pre-trained model via minimizing the ACL loss  $\mathcal{L}_{\text{ACL}}(S^*)$  achieve the minimized  $\mathcal{L}_{\text{RD}}(U)$ , thus helping attain adversarially robust presentations, which could be beneficial to the robustness and standard transferability.

To solve Eq. (3), we follow previous works (Killamsetty et al., 2021b;c), modifying Eq. (3) by conducting one-step gradient approximation as the first step, i.e.,

$$S^* = \arg \min_{S \subseteq X, |S|/|X| \leq k} \mathcal{L}_{\text{RD}}(U; \theta - \eta \nabla_{\theta} \mathcal{L}_{\text{ACL}}(S; \theta)), \quad (4)$$

where  $\eta > 0$  is the learning rate. We define a set function  $G : 2^X \rightarrow \mathbb{R}$  as follows:

$$G_{\theta}(S \subseteq X) \triangleq -\mathcal{L}_{\text{RD}}(U; \theta - \eta \nabla_{\theta} \mathcal{L}_{\text{ACL}}(S; \theta)). \quad (5)$$

Similar to Killamsetty et al. (2021b;c), we fix the size of the coreset, i.e.,  $|S^*| = k|X|$  being a constant. Then, the optimization problem in Eq. (3) can be reformulated as

$$S^* = \arg \max_{S \subseteq X, |S|/|X|=k} G_{\theta}(S). \quad (6)$$

### 3.3 Method—Greedy Search

Eq. (6) is formulated as a problem of maximizing a set function subject to a cardinality constraint (Karp, 1972; Killamsetty et al., 2021b;c). A naive solution to this problem is to traverse all possible subsets of size  $kN$  and select the subset  $S$  which has the largest value  $G_{\theta}(S)$ . But this naive solution is computationally prohibitive since it needs to calculate the loss gradient  $\nabla_{\theta} \mathcal{L}_{\text{ACL}}(S; \theta)$  for  $\binom{N}{kN}$  times. Fortunately, Das and Kempe (2011) and Gatmiry and Gomez-Rodriguez (2021) proposed the greedy search algorithm to efficiently solve this kind of problem approximately if the set function is monotone and  $\gamma$ -weakly submodular. Note that the greedy search algorithm shown in Algorithm 1 only needs to calculate the loss gradient  $\lceil N/\beta \rceil + \lfloor kN/\beta \rfloor \ll \binom{N}{kN}$  times where  $\beta$  is batch size.

**Definition 1** (Monotonicity and  $\gamma$ -weakly submodularity (Das and Kempe, 2011)). *Given a set function  $G : 2^X \rightarrow \mathbb{R}$ , the marginal gain of  $G$  is defined as  $G(x|A) \triangleq G(A \cup \{x\}) - G(A)$  for any  $A \subset X$  and  $x \in X \setminus A$ . The function  $G$  is monotone if  $G(x|A) \geq 0$  for any  $A \subset X$  and  $x \in X \setminus A$ . The function  $G$  is called  $\gamma$ -weakly submodular if  $\sum_{x \in B \setminus A} G(x|A) \geq \gamma[G(A \cup B) - G(A)]$  for some  $\gamma \in (0, 1]$  and any subset  $A \subset B \subseteq X$ .*

**Assumption 1.** The first-order gradients and the second-order gradients of  $\ell_{\text{RD}}$  and  $\ell_{\text{ACL}}$  are bounded w.r.t.  $\theta$ , i.e.,

$$\begin{aligned} \left\| \frac{\partial}{\partial \theta} \ell_{\text{RD}}(x; \theta) \right\| &\leq L_1, \left\| \frac{\partial}{\partial \theta} \ell_{\text{ACL}}(x; \theta) \right\| \leq L_2, \\ \left\| \frac{\partial^2}{\partial \theta^2} \ell_{\text{RD}}(x; \theta) \right\| &\leq L_3, \left\| \frac{\partial^2}{\partial \theta^2} \ell_{\text{ACL}}(x; \theta) \right\| \leq L_4, \end{aligned}$$

where  $L_1, L_2, L_3$ , and  $L_4$  are positive constants.

Next, we theoretically show that a proxy set function  $\hat{G}_\theta(S)$  is monotone and  $\gamma$ -weakly submodular in Theorem 1.

**Theorem 1.** We define a proxy set function  $\hat{G}_\theta(S) \triangleq G_\theta(S) + |S|\sigma$ , where  $\sigma = 1 + \nu_1 + \nu_2 L_2 + \eta M L_2 (L_1 + \eta k N (L_1 L_4 + L_2 L_3))$ ,  $\nu_1 \rightarrow 0^+$ , and  $\nu_2 > 0$  are positive constants. Given Assumption 1,  $\hat{G}_\theta(S)$  is monotone and  $\gamma$ -weakly submodular where  $\gamma > \gamma^* = \frac{1}{2\sigma-1}$ .

The proof is in Appendix A.1. We construct a proxy optimization problem in Eq. (6) as follows:

$$\hat{S}^* = \arg \max_{S \subseteq X, |S|/|X|=k} \hat{G}_\theta(S). \quad (7)$$

According to Theorem 1, a greedy search algorithm (Das and Kempe, 2011; Gatmiry and Gomez-Rodriguez, 2021) can be leveraged to approximately solve the proxy problem in Eq. (7) and it can provide the following optimality guarantee of the optimization problem in Eq. (6).

**Theorem 2.** Given a fixed parameter  $\theta$ , we denote the optimal solution of Eq. (6) as  $G_\theta^* = \sup_{S \subseteq X, |S|/|X|=k} G_\theta(S)$ . Then,  $\hat{S}^*$  in Eq. (7) found via greedy search satisfies

$$G_\theta(\hat{S}^*) \geq G_\theta^* - (G_\theta^* + kN\sigma) \cdot e^{-\gamma^*}.$$

**Remark.** The proof is in Appendix A.2. Theorem 2 indicates that the greedy search for solving the proxy problem in Eq. (7) can provide a guaranteed lower-bound of the original problem in Eq. (6), which implies that RCS via greedy search can help ACL to obtain the minimized RD and robust representations. We also empirically validate that ACL on the coreset selected by RCS can achieve a lower RD compared with ACL on the randomly selected subset in Figure 3, which empirically supports that RCS via greedy search is effective in achieving the minimized RD.

**Algorithm of RCS.** Therefore, we use a greedy search algorithm via batch-wise selection for RCS. Algorithm 1 iterates the batch-wise selection  $\lfloor k|X|/\beta \rfloor$  times. At each iteration, it finds the minibatch  $B$  that has the largest gain  $\hat{G}_\theta(B|S)$  based on the parameters updated by the previously selected coreset, and then adds this minibatch into the final coreset. RCS via greedy search needs to calculate the gradient for each minibatch  $\lceil N/\beta \rceil$  times (Line 6 in Algorithm 1) and the gradient on the validation set  $\lfloor kN/\beta \rfloor$  times (Line 10 in Algorithm 1). In total, RCS needs to calculate the loss gradient  $\lceil N/\beta \rceil + \lfloor kN/\beta \rfloor \ll \binom{N}{kN}$  times, which is significantly more efficient than the native solution. Similar to Killamsetty et al. (2021b;c), we approximate the marginal gain function using the Taylor expansion as follows:

$$\hat{G}_\theta(B|S) \approx \eta \nabla_\theta \mathcal{L}_{\text{RD}}(U; \theta_S)^\top \nabla_\theta \mathcal{L}_{\text{ACL}}(B; \theta) + \sigma,$$

where  $\theta_S = \theta - \eta \nabla_\theta \mathcal{L}_{\text{ACL}}(S; \theta)$  and  $B$  is a minibatch. It enables us to efficiently calculate the marginal gain for each minibatch (Line 13 in Algorithm 1). Since  $\sigma$  is a constant, we omit this term in Algorithm 1.

### 3.4 Efficient ACL via RCS

We show an efficient ACL procedure via RCS in Algorithm 2. ACL with RCS trains the model on the previously selected coreset for  $\lambda \in \mathbb{N}$  epochs, and for every  $\lambda$  epochs a new coreset is selected. The pre-training procedure is repeated until the required epoch  $E \in \mathbb{N}$  is reached. Then, we provide three tricks to make RCS effective and efficient as well as an extra trick to enable efficient RCS on large-scale datasets with limited GPU memory in Appendix B.1.

**Warmup on the entire training set.** We take  $\omega$  epochs to train the model on the entire training set as a warm start, similar to Killamsetty et al. (2021a;b;c). Warmup training enables the model to have a good starting point to provide informative gradients used for RCS.

**Last-layer gradients.** It is computationally expensive to compute the gradients over full layers of a deep model due to a tremendous number of parameters in the model. To tackle this issue, we utilize a last-layer gradient approximation, similar to Killamsetty et al. (2021b;c), by only considering the loss gradients of the projection head  $g$  during RCS. Note that we still update all the parameters during ACL.

---

**Algorithm 1** Robustness-aware coreset selection (RCS)

---

```
1: Input: Unlabeled training set  $X$ , unlabeled validation set  $U$ , batch size  $\beta$ , model  $g \circ f_\theta$ , learning rate for RCS  $\eta$ , subset fraction  $k \in (0, 1]$ 
2: Output: Coreset  $S$ 
3: Initialize  $S \leftarrow \emptyset$ 
4: Split entire set into minibatches  $X = \{B_m\}_{m=1}^{\lceil |X|/\beta \rceil}$ 
5: for each minibatch  $B_m \in X$  do
6:   Compute gradient  $q_m \leftarrow \nabla_\theta \mathcal{L}_{\text{ACL}}(B_m; \theta)$ 
7: end for
8: // Conduct greedy search via batch-wise selection
9: for  $1, \dots, \lfloor k|X|/\beta \rfloor$  do
10:  Compute gradient  $q_U \leftarrow \nabla_\theta \mathcal{L}_{\text{RD}}(U; \theta)$ 
11:  Initialize  $best\_gain = -\infty$ 
12:  for each minibatch  $B_m \in X$  do
13:    Compute marginal gain  $\hat{G}(B_m|S) \leftarrow \eta q_U^\top q_m$ 
14:    if  $\hat{G}(B_m|S) > best\_gain$  then
15:      Update  $s \leftarrow m, best\_gain \leftarrow \hat{G}(B_m|S)$ 
16:    end if
17:  end for
18:  Update  $S \leftarrow S \cup B_s, X \leftarrow X \setminus B_s$ 
19:  Update  $\theta \leftarrow \theta - \eta q_s$ 
20: end for
```

---

---

**Algorithm 2** Efficient ACL via RCS

---

```
1: Input: Unlabeled training set  $X$ , unlabeled validation set  $U$ , total training epochs  $E$ , learning rate  $\eta'$ , batch size  $\beta$ , warmup epoch  $\omega$ , epoch interval for executing RCS  $\lambda$ , subset fraction  $k$ , learning rate for RCS  $\eta$ 
2: Output: robust pre-trained feature extractor  $f_\theta$ 
3: Initialize parameters of model  $g \circ f_\theta$ 
4: Initialize training set  $S \leftarrow X$ 
5: for  $e = 0$  to  $E - 1$  do
6:   if  $e \% \lambda == 0$  and  $e \geq \omega$  then
7:      $S \leftarrow \text{RCS}(X, U, \beta, g \circ f_\theta, \eta, k)$  //by Algorithm 1
8:   end if
9:   for batch  $m = 1, \dots, \lceil |S|/\beta \rceil$  do
10:    Sample a minibatch  $B_m$  from  $S$ 
11:    Update  $\theta \leftarrow \theta - \eta' \mathcal{L}_{\text{ACL}}(B_m; \theta)$ 
12:   end for
13: end for
```

---

**Adversarial data approximation.** Calculating adversarial data during CS is extremely time-consuming since generating adversarial data needs to iteratively perform BP  $T$  times. We let  $T_{\text{ACL}}$  be PGD steps,  $\epsilon_{\text{ACL}}$  be the adversarial budget, and  $\rho_{\text{ACL}}$  be the step size for PGD during ACL. Similarly,  $T_{\text{RCS}}$ ,  $\epsilon_{\text{RCS}}$ , and  $\rho_{\text{RCS}}$  denote PGD configurations during RCS. To mitigate the above issue, we decrease  $T_{\text{RCS}}$  (i.e.,  $0 < T_{\text{RCS}} \leq T_{\text{ACL}}$ ) and  $\rho_{\text{RCS}} = \frac{\rho_{\text{ACL}} T_{\text{ACL}}}{T_{\text{RCS}}}$  for efficiently generating adversarial data during CS, similar to ACS (Dolatbadi et al., 2022). Note that the same adversarial budget is used for ACL and RCS, i.e.,  $\epsilon_{\text{RCS}} = \epsilon_{\text{ACL}}$ .

## 4 Experiments

In this section, we first validate that our proposed RCS can significantly accelerate ACL (Jiang et al., 2020) on CIFAR-10 (Krizhevsky, 2009) with minor degradation in robustness transferability and standard transferability to downstream tasks. Then, we show that RCS is compatible with supervised AT as well. At last, we apply RCS to a large-scale dataset, i.e., ImageNet-1K (Deng et al., 2009) to demonstrate that RCS enhances the scalability of ACL.

### 4.1 Efficient ACL on CIFAR-10

**Experimental configurations.** We pre-trained ResNet-18 (He et al., 2016) on CIFAR-10 vis ACL using SGD for 1000 epochs with an initial learning rate 5.0 and a cosine annealing scheduler (Loshchilov and Hutter, 2016), following Jiang

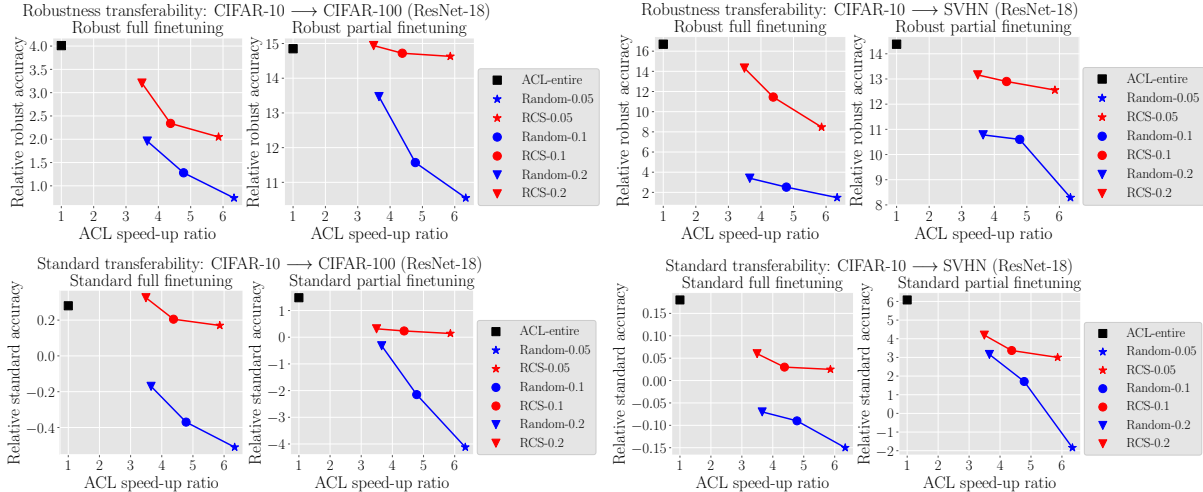


Figure 2: Transferability from CIFAR-10 to CIFAR-100 and SVHN of ACL pre-trained ResNet-18 with various CS strategies. “ACL-entire” denotes ACL on the entire training set of CIFAR-10. The number after the dash line denotes subset fraction  $k \in \{0.05, 0.1, 0.2\}$ .

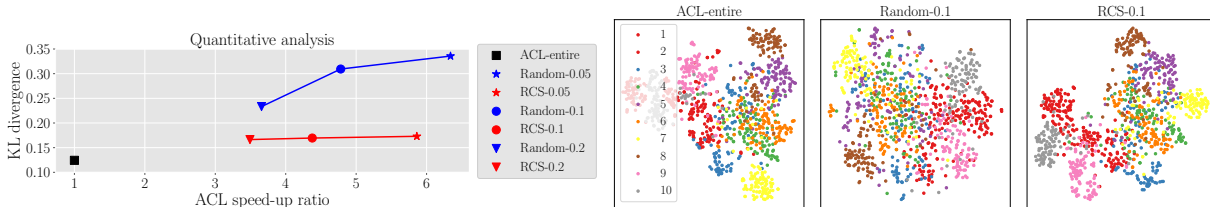


Figure 3: Leftmost panel: Average value of the KL divergence between natural CIFAR-10 test data and its adversarial variant. Right three panels: Feature representations visualized via t-SNE.

et al. (2020). We set  $\beta = 512$ ,  $T_{\text{ACL}} = 5$ ,  $\epsilon_{\text{ACL}} = 8/255$ ,  $\rho_{\text{ACL}} = 2/255$ , and  $T_{\text{RCS}} = 3$ . We took  $\omega = 100$  epochs for warmup, and then CS was executed every  $\lambda = 20$  epochs. We used different subset fractions  $k \in \{0.05, 0.1, 0.2\}$  for CS. The KL divergence was used as the distance function to calculate  $\mathcal{L}_{\text{RD}}(\cdot)$  for all the experiments in Section 4. We show the experimental details regarding robust finetuning and standard finetuning in Appendix B.2. We repeated all the experiments using different random seeds three times and report the median results to exclude the effect of randomization. We also provide the results of RCS using the JS divergence and the OT distance in Appendix B.5, RCS with various warmup epochs  $\omega \in \{100, 200, 300\}$  in Appendix B.6, and RCS for a variant of the ACL method (Fan et al., 2021) in Appendix B.7.

**Baseline.** We replaced RCS (Line 7 in Algorithm 2) with the random selection strategy (dubbed as “Random”) to obtain the coreset  $S$  during ACL as the baseline. The implementation of Random exactly follows that in the coreset and data selection library (Killamsetty et al., 2021b).

**Speed-up ratio.** The *speed-up ratio* denotes the ratio of the running time of ACL on the entire set (dubbed as “ACL-entire”) to that of ACL with various CS strategies. We report the running time of ACL-entire in Table 7.

**Relative standard/robust accuracy.** *Relative standard/robust accuracy* refers to the standard/robust test accuracy achieved by adversarially pre-trained models minus that achieved by standardly pre-trained models on downstream tasks after standard/robust finetuning procedure. The higher the relative standard/robust accuracy is, the better adversarially pre-trained model’s standard/robustness transferability is compared with standardly pre-trained models. We report the standard and robust test accuracy on downstream tasks achieved by standardly pre-trained models in Tables 3–6 for checking the absolute test accuracy on downstream tasks. To evaluate the robust test accuracy, we generated adversarial test data via PGD with 20 PGD steps, adversarial budget  $8/255$ , and step size  $2/255$  (dubbed as “PGD-20”). We also show the robust test accuracy evaluated by AutoAttack (Croce and Hein, 2020) in Appendix B.4.

**Effectiveness of RCS in efficient ACL.** Figure 2 demonstrates the robustness transferability (upper panels) and standard transferability (lower panels) from CIFAR-10 to downstream tasks (i.e., CIFAR-100 and SVHN (Netzer et al., 2011)) of pre-trained ResNet-18. We observe that ACL with RCS (red lines) always shows significantly better



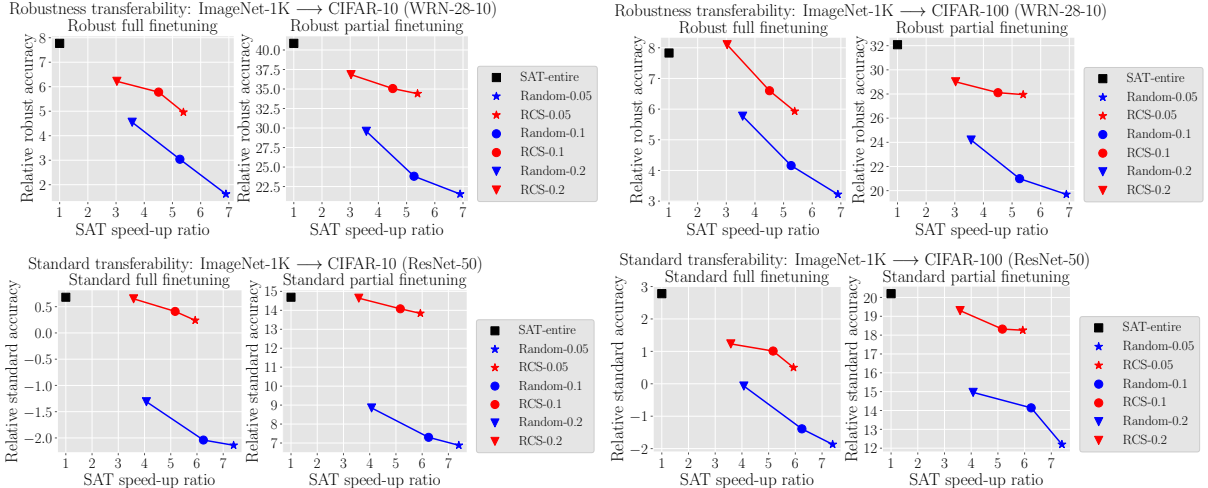


Figure 4: Transferability from ImageNet-1K to CIFAR-10 and CIFAR-100 of SAT pre-trained models with various CS strategies. “SAT-entire” denotes SAT on the entire training set of ImageNet-1K. The number after the dash line denotes subset fraction  $k \in \{0.05, 0.1, 0.2\}$ .

transferability than ACL with Random (blue lines) among various subset fractions. In addition, we can find that the extra computation incurred by the greedy search of RCS is almost negligible since the speed-up ratio of ACL with RCS is almost the same as that of ACL with Random. Compared with ACL-entire (black square), ACL with RCS only slightly hurts transferability. Meanwhile, ACL with RCS always gains improved standard and robust accuracies on downstream tasks compared with standard CL pre-training (Chen et al., 2020). It demonstrates that RCS is a principled method to speed up ACL with minor degradation in the transferability of adversarially pre-trained models.

**Quantitative analysis.** We collected the average value of the KL divergence between natural data point  $x$  and its PGD-20 adversarial variant on the CIFAR-10 test set (i.e.,  $\ell_{RD}(x)$ ) and show it in the leftmost panel of Figure 3. It validates that RCS helps minimize RD, thus helping ACL obtain useful and adversarially robust representations. Besides, we also demonstrate feature representations of ResNet-18 pre-trained via ACL with different CS strategies using t-SNE (Van der Maaten and Hinton, 2008) in the right three panels of Figure 3. This shows that ACL with RCS can achieve a more clear class separation compared with ACL with Random, thus providing better transferability (Fan et al., 2021). Extensive visualizations are shown in Appendix B.8 due to the limited space. Our quantitative analysis further validates the effectiveness of RCS in speeding up ACL while helping efficient ACL yield useful and robust representations.

## 4.2 Compatibility with Supervised Adversarial Training (AT)

In this subsection, we empirically validate that RCS is compatible with two typical kinds of supervised AT, i.e., SAT (Madry et al., 2018) and TRADES (Zhang et al., 2019). Following Hendrycks et al. (2019), we pre-trained WideResNet (Zagoruyko and Komodakis, 2016) with width 10 and depth 28 (WRN-28-10) on ImageNet-1K of  $32 \times 32$  resolution via SAT with RCS and show robustness transferability to CIFAR-10 and CIFAR-100 in the upper panels of Figure 4. Following Salman et al. (2020), we pre-trained ResNet-50 on ImageNet-1K of  $224 \times 224$  resolution via SAT with RCS and demonstrate standard transferability to downstream tasks in the lower panels of Figure 4. The details of experimental configurations are in Appendix B.9. We also provide the comparison between RCS and ACS (Dolatabadi et al., 2022) for efficient supervised AT on CIFAR-10 in Appendix B.9.

Figure 4 shows that RCS can accelerate SAT on ImageNet-1K by 4–6 times. Besides, SAT with RCS always obtains much better transferability than SAT with Random and consistently achieves better transferability than standard pre-training as well. It validates that RCS is an effective method for efficient supervised AT. Thus, RCS can be regarded as a unified framework for efficient robust pre-training.

## 4.3 Benchmarks on ImageNet-1K

to the best of our knowledge, we are the first to apply ACL (Jiang et al., 2020) on ImageNet-1K (Deng et al., 2009) efficiently via RCS. As shown in Table 1, ACL on the entire training set of ImageNet-1K will need about 650.2 hours using 4 NVIDIA RTX A5000 GPUs, which is extremely time-consuming and unmanageable for us to conduct ACL on the entire set. Thus, we do not provide the results of ACL on the entire set.

Table 1: The test accuracy evaluated on CIFAR-10 of pre-trained WRN-28-10 models after finetuning procedure. Pre-trained WRN-28-10 models are trained on ImageNet-1K via standard CL (Chen et al., 2020), ACL with Random, and ACL with RCS, respectively.

Pre-training	Runing time (hours)	Standard test accuracy		Robust test accuracy	
		Standard full finetuning	Standard partial finetuning	Robust full finetuning	Robust partial finetuning
Standard CL	147.4	95.69%	80.93%	51.15%	10.00%
ACL on entire set	650.2	-	-	-	-
ACL with Random	94.3	96.06%	81.08%	53.37%	33.91%
ACL with RCS	111.8	<b>96.24%</b>	<b>82.01%</b>	<b>55.25%</b>	<b>36.13%</b>

Table 2: The test accuracy evaluated on CIFAR-100 of pre-trained WRN-28-10 models after finetuning procedure. Pre-trained WRN-28-10 models are trained on ImageNet-1K via standard CL (Chen et al., 2020), ACL with Random, and ACL with RCS, respectively.

Pre-training	Runing time (hours)	Standard test accuracy		Robust test accuracy	
		Standard full finetuning	Standard partial finetuning	Robust full finetuning	Robust partial finetuning
Standard CL	147.4	79.94%	55.47%	29.23%	1.08%
ACL on entire set	650.2	-	-	-	-
ACL with Random	94.3	80.33%	55.51%	30.17%	17.24%
ACL with RCS	111.8	<b>80.96%</b>	<b>56.43%</b>	<b>32.29%</b>	<b>19.37%</b>

We pre-trained WRN-28-10 on ImageNet-1K of  $32 \times 32$  resolution via ACL (Jiang et al., 2020) with RCS and Random, respectively. We set  $\beta = 512$ ,  $T_{ACL} = 5$ ,  $\epsilon_{ACL} = 8/255$ ,  $\rho_{ACL} = 2/255$ , and  $T_{RCS} = 1$ . The temperature parameter  $t$  was set as 0.1, following Chen et al. (2020). The model was trained using SGD for 200 epochs with an initial learning rate 0.6 and a cosine annealing scheduler. We set warmup epoch  $\omega = 20$ , and then CS was executed every  $\lambda = 10$  epochs. We pre-trained WRN-28-10 with the subset fraction  $k = 0.05$  and then finetuned it on CIFAR-10 and CIFAR-100. Details of finetuning procedure are in Appendix B.2.

Tables 1 and 2 demonstrate the transferability of pre-trained WRN-32-10 from ImageNet-1K to CIFAR-10 and CIFAR-100, respectively. The two tables show that ACL with RCS consistently leads to better robust and standard test accuracy on downstream tasks than ACL with Random. Besides, we can observe that ACL with RCS often obtains better robustness and standard transferability compared with standard CL. Surprisingly, ACL with RCS even consumed less running time (111.8 hours) than standard CL (147.4 hours) while achieving better transferability. It validates that RCS effectively enhances the scalability of ACL, and efficient ACL via RCS can yield useful and robust representations.

## 5 Conclusion

This paper proposed a robustness-aware coreset selection (RCS) framework for accelerating robust pre-training. RCS found an informative subset that helps minimize the representational divergence between natural data and their adversarial counterparts. We theoretically showed that RCS can be efficiently solved by greedy search approximately with an optimality guarantee. RCS does not require label information and is thus applicable to ACL as well as supervised AT. Our experimental results validated that RCS can significantly speed up both ACL and supervised AT while slightly hurting the robustness and standard transferability. Future research includes (a) how to incorporate RCS with FGSM (Goodfellow et al., 2014; Wong et al., 2020) to further speed up ACL on ImageNet-1K, (b) how to adapt RCS to accelerate semi-supervised AT (Alayrac et al., 2019).

## Acknowledgements

Jingfeng Zhang was supported by JST ACT-X Grant Number JPMJAX21AF and JSPS KAKENHI Grant Number 22K17955, Japan. Masashi Sugiyama was supported by the Institute for AI and Beyond, UTokyo, Japan. Mohan Kankanhalli’s research is supported by the National Research Foundation, Singapore under its Strategic Capability Research Centres Funding Initiative. Any opinions, findings and conclusions or recommendations expressed in this material are those of the author(s) and do not reflect the views of National Research Foundation, Singapore.

## References

- Jia Deng, Wei Dong, Richard Socher, Li-Jia Li, Kai Li, and Li Fei-Fei. Imagenet: A large-scale hierarchical image database. In *2009 IEEE conference on computer vision and pattern recognition*, pages 248–255. Ieee, 2009.
- Tal Ridnik, Emanuel Ben-Baruch, Asaf Noy, and Lihi Zelnik-Manor. Imagenet-21k pretraining for the masses. *arXiv preprint arXiv:2104.10972*, 2021.
- Alexey Dosovitskiy, Lucas Beyer, Alexander Kolesnikov, Dirk Weissenborn, Xiaohua Zhai, Thomas Unterthiner, Mostafa Dehghani, Matthias Minderer, Georg Heigold, Sylvain Gelly, et al. An image is worth 16x16 words: Transformers for image recognition at scale. *arXiv preprint arXiv:2010.11929*, 2020.
- Alex Krizhevsky. Learning multiple layers of features from tiny images. Technical report, 2009.
- Xiaohua Zhai, Joan Puigcerver, Alexander Kolesnikov, Pierre Ruysen, Carlos Riquelme, Mario Lucic, Josip Djolonga, Andre Susano Pinto, Maxim Neumann, Alexey Dosovitskiy, et al. A large-scale study of representation learning with the visual task adaptation benchmark. *arXiv preprint arXiv:1910.04867*, 2019.
- Rishi Bommasani, Drew A Hudson, Ehsan Adeli, Russ Altman, Simran Arora, Sydney von Arx, Michael S Bernstein, Jeannette Bohg, Antoine Bosselut, Emma Brunskill, et al. On the opportunities and risks of foundation models. *arXiv preprint arXiv:2108.07258*, 2021.
- Tom Brown, Benjamin Mann, Nick Ryder, Melanie Subbiah, Jared D Kaplan, Prafulla Dhariwal, Arvind Neelakantan, Pranav Shyam, Girish Sastry, Amanda Askell, et al. Language models are few-shot learners. *Advances in neural information processing systems*, 33:1877–1901, 2020.
- Benjamin Elizalde, Soham Deshmukh, Mahmoud Al Ismail, and Huaming Wang. Clap: Learning audio concepts from natural language supervision. *arXiv preprint arXiv:2206.04769*, 2022.
- Xinlei Chen and Kaiming He. Exploring simple siamese representation learning. In *Proceedings of the IEEE/CVF Conference on Computer Vision and Pattern Recognition*, pages 15750–15758, 2021.
- Phuc H Le-Khac, Graham Healy, and Alan F Smeaton. Contrastive representation learning: A framework and review. *IEEE Access*, 8:193907–193934, 2020.
- Ting Chen, Simon Kornblith, Mohammad Norouzi, and Geoffrey Hinton. A simple framework for contrastive learning of visual representations. In *International conference on machine learning*, pages 1597–1607. PMLR, 2020.
- Ziyu Jiang, Tianlong Chen, Ting Chen, and Zhangyang Wang. Robust pre-training by adversarial contrastive learning. *Advances in Neural Information Processing Systems*, 33:16199–16210, 2020.
- Lijie Fan, Sijia Liu, Pin-Yu Chen, Gaoyuan Zhang, and Chuang Gan. When does contrastive learning preserve adversarial robustness from pretraining to finetuning? *Advances in Neural Information Processing Systems*, 34: 21480–21492, 2021.
- Hadi Salman, Andrew Ilyas, Logan Engstrom, Ashish Kapoor, and Aleksander Madry. Do adversarially robust imagenet models transfer better? *Advances in Neural Information Processing Systems*, 33:3533–3545, 2020.
- Xiaojun Xu, Jacky Y Zhang, Evelyn Ma, Hyun Ho Son, Sanmi Koyejo, and Bo Li. Adversarially robust models may not transfer better: Sufficient conditions for domain transferability from the view of regularization. In *International Conference on Machine Learning*, pages 24770–24802. PMLR, 2022.
- Eric Wong, Leslie Rice, and J. Zico Kolter. Fast is better than free: Revisiting adversarial training. In *ICLR*, 2020.
- Ali Shafahi, Mahyar Najibi, Mohammad Amin Ghiasi, Zheng Xu, John Dickerson, Christoph Studer, Larry S Davis, Gavin Taylor, and Tom Goldstein. Adversarial training for free! In *NeurIPS*, 2019.
- Dan Feldman. Core-sets: Updated survey. In *Sampling techniques for supervised or unsupervised tasks*, pages 23–44. Springer, 2020.
- Baharan Mirzasoleiman, Jeff Bilmes, and Jure Leskovec. Coresets for data-efficient training of machine learning models. In *International Conference on Machine Learning*, pages 6950–6960. PMLR, 2020.
- Krishnateja Killamsetty, S Durga, Ganesh Ramakrishnan, Abir De, and Rishabh Iyer. Grad-match: Gradient matching based data subset selection for efficient deep model training. In *International Conference on Machine Learning*, pages 5464–5474. PMLR, 2021a.
- Krishnateja Killamsetty, Durga Sivasubramanian, Ganesh Ramakrishnan, and Rishabh Iyer. Glisten: Generalization based data subset selection for efficient and robust learning. In *Proceedings of the AAAI Conference on Artificial Intelligence*, volume 35, pages 8110–8118, 2021b.
- Krishnateja Killamsetty, Xujiang Zhao, Feng Chen, and Rishabh Iyer. Retrieve: Coreset selection for efficient and robust semi-supervised learning. *Advances in Neural Information Processing Systems*, 34:14488–14501, 2021c.

- Hadi M Dolatabadi, Sarah Erfani, and Christopher Leckie. Adversarial coreset selection for efficient robust training. *arXiv preprint arXiv:2209.05785*, 2022.
- Aleksander Madry, Aleksandar Makelov, Ludwig Schmidt, Dimitris Tsipras, and Adrian Vladu. Towards deep learning models resistant to adversarial attacks. In *ICLR*, 2018.
- Hongyang Zhang, Yaodong Yu, Jiantao Jiao, Eric P. Xing, Laurent El Ghaoui, and Michael I. Jordan. Theoretically principled trade-off between robustness and accuracy. In *ICML*, 2019.
- Takeru Miyato, Shin-ichi Maeda, Masanori Koyama, and Shin Ishii. Virtual adversarial training: a regularization method for supervised and semi-supervised learning. *IEEE transactions on pattern analysis and machine intelligence*, 41(8):1979–1993, 2018.
- Abhimanyu Das and David Kempe. Submodular meets spectral: Greedy algorithms for subset selection, sparse approximation and dictionary selection. In *ICML*, 2011.
- Khashayar Gatmiry and Manuel Gomez-Rodriguez. The network visibility problem. *ACM Transactions on Information Systems (TOIS)*, 40(2):1–42, 2021.
- Gregory Koch, Richard Zemel, Ruslan Salakhutdinov, et al. Siamese neural networks for one-shot image recognition. In *ICML deep learning workshop*, volume 2, page 0. Lille, 2015.
- Minseon Kim, Jihoon Tack, and Sung Ju Hwang. Adversarial self-supervised contrastive learning. *Advances in Neural Information Processing Systems*, 33:2983–2994, 2020.
- Chih-Hui Ho and Nuno Vasconcelos. Contrastive learning with adversarial examples. *Advances in Neural Information Processing Systems*, 33:17081–17093, 2020.
- Qiyang Yu, Jieming Lou, Xianyuan Zhan, Qizhang Li, Wangmeng Zuo, Yang Liu, and Jingjing Liu. Adversarial contrastive learning via asymmetric infonce. In *European Conference on Computer Vision*, pages 53–69. Springer, 2022.
- Chaoning Zhang, Kang Zhang, Chenshuang Zhang, Axi Niu, Jiu Feng, Chang D Yoo, and In So Kweon. Decoupled adversarial contrastive learning for self-supervised adversarial robustness. In *European Conference on Computer Vision*, pages 725–742. Springer, 2022a.
- Ian J Goodfellow, Jonathon Shlens, and Christian Szegedy. Explaining and harnessing adversarial examples. *arXiv preprint arXiv:1412.6572*, 2014.
- Maksym Andriushchenko and Nicolas Flammarion. Understanding and improving fast adversarial training. *Advances in Neural Information Processing Systems*, 33:16048–16059, 2020.
- Yihua Zhang, Guanhua Zhang, Prashant Khanduri, Mingyi Hong, Shiyu Chang, and Sijia Liu. Revisiting and advancing fast adversarial training through the lens of bi-level optimization. In *International Conference on Machine Learning*, pages 26693–26712. PMLR, 2022b.
- Dan Hendrycks, Kimin Lee, and Mantas Mazeika. Using pre-training can improve model robustness and uncertainty. In *International Conference on Machine Learning*, pages 2712–2721. PMLR, 2019.
- Haichao Zhang and Jianyu Wang. Defense against adversarial attacks using feature scattering-based adversarial training. *Advances in Neural Information Processing Systems*, 32, 2019.
- Sravanti Addepalli, Samyak Jain, and R Venkatesh Babu. Efficient and effective augmentation strategy for adversarial training. *arXiv preprint arXiv:2210.15318*, 2022.
- Richard M Karp. Reducibility among combinatorial problems. In *Complexity of computer computations*, pages 85–103. Springer, 1972.
- Kaiming He, Xiangyu Zhang, Shaoqing Ren, and Jian Sun. Deep residual learning for image recognition. In *Proceedings of the IEEE conference on computer vision and pattern recognition*, pages 770–778, 2016.
- Ilya Loshchilov and Frank Hutter. Sgdr: Stochastic gradient descent with warm restarts. *arXiv preprint arXiv:1608.03983*, 2016.
- Francesco Croce and Matthias Hein. Reliable evaluation of adversarial robustness with an ensemble of diverse parameter-free attacks. In *International conference on machine learning*, pages 2206–2216. PMLR, 2020.
- Yuval Netzer, Tao Wang, Adam Coates, Alessandro Bissacco, Bo Wu, and Andrew Y Ng. Reading digits in natural images with unsupervised feature learning. 2011.
- Laurens Van der Maaten and Geoffrey Hinton. Visualizing data using t-sne. *Journal of machine learning research*, 9(11), 2008.
- Sergey Zagoruyko and Nikos Komodakis. Wide residual networks. *arXiv preprint arXiv:1605.07146*, 2016.

- Jean-Baptiste Alayrac, Jonathan Uesato, Po-Sen Huang, Alhussein Fawzi, Robert Stanforth, and Pushmeet Kohli. Are labels required for improving adversarial robustness? *Advances in Neural Information Processing Systems*, 32, 2019.
- Cihang Xie, Mingxing Tan, Boqing Gong, Jiang Wang, Alan L Yuille, and Quoc V Le. Adversarial examples improve image recognition. In *Proceedings of the IEEE/CVF Conference on Computer Vision and Pattern Recognition*, pages 819–828, 2020.
- Anish Athalye, Nicholas Carlini, and David Wagner. Obfuscated gradients give a false sense of security: Circumventing defenses to adversarial examples. In *International conference on machine learning*, pages 274–283. PMLR, 2018.

## A Theoretical Analysis

### A.1 Proof of Theorem 1

**Theorem 1 (Restated)** We define a proxy set function  $\hat{G}_\theta(S) \triangleq G_\theta(S) + |S|\sigma$ , where  $\sigma = 1 + \nu_1 + \nu_2 L_2 + \eta M L_2(L_1 + \eta k N(L_1 L_4 + L_2 L_3))$ ,  $\nu_1 \rightarrow 0^+$ , and  $\nu_2 > 0$  are positive constants. Given Assumption 1,  $\hat{G}_\theta(S)$  is monotone and  $\gamma$ -weakly submodular where  $\gamma > \gamma^* = \frac{1}{2\sigma-1}$ .

*Proof.* We first provide **proof of monotonicity of  $\hat{G}_\theta(S)$** . We use Taylor expansion two times to convert the marginal gain function  $\hat{G}_\theta(x|S)$  as follows,

$$\begin{aligned}
\hat{G}_\theta(x|S) &= \hat{G}_\theta(S \cup \{x\}) - \hat{G}_\theta(S) \\
&= -\mathcal{L}_{\text{RD}}(U; \theta - \eta \frac{\partial}{\partial \theta} \mathcal{L}_{\text{ACL}}(S; \theta) - \eta \frac{\partial}{\partial \theta} \mathcal{L}_{\text{ACL}}(\{x\}; \theta)) + \mathcal{L}_{\text{RD}}(U; \theta - \eta \frac{\partial}{\partial \theta} \mathcal{L}_{\text{ACL}}(S; \theta)) + \sigma \\
&\stackrel{\text{Taylor expansion}}{=} \eta \frac{\partial}{\partial \theta} \mathcal{L}_{\text{RD}}(U; \theta - \eta \frac{\partial}{\partial \theta} \mathcal{L}_{\text{ACL}}(S; \theta))^\top \frac{\partial}{\partial \theta} \mathcal{L}_{\text{ACL}}(\{e\}; \theta) + \xi_1(\theta) + \sigma \\
&\stackrel{\text{Taylor expansion}}{=} \eta \frac{\partial}{\partial \theta} \left[ \mathcal{L}_{\text{RD}}(U; \theta) - \eta \frac{\partial}{\partial \theta} \mathcal{L}_{\text{RD}}(U; \theta)^\top \frac{\partial}{\partial \theta} \mathcal{L}_{\text{ACL}}(S; \theta) + \xi_2(\theta) \right]^\top \frac{\partial}{\partial \theta} \mathcal{L}_{\text{ACL}}(\{x\}; \theta) \\
&\quad + \xi_1(\theta) + \sigma \\
&= \eta \frac{\partial}{\partial \theta} \mathcal{L}_{\text{RD}}(U; \theta)^\top \frac{\partial}{\partial \theta} \mathcal{L}_{\text{ACL}}(\{x\}; \theta) - \eta^2 \frac{\partial}{\partial \theta} \mathcal{L}_{\text{RD}}(U; \theta)^\top \frac{\partial^2}{\partial \theta^2} \mathcal{L}_{\text{ACL}}(S; \theta) \frac{\partial}{\partial \theta} \mathcal{L}_{\text{ACL}}(\{x\}; \theta) \\
&\quad - \eta^2 \frac{\partial}{\partial \theta} \mathcal{L}_{\text{ACL}}(S; \theta)^\top \frac{\partial^2}{\partial \theta^2} \mathcal{L}_{\text{RD}}(U; \theta) \frac{\partial}{\partial \theta} \mathcal{L}_{\text{ACL}}(\{x\}; \theta) + \frac{\partial}{\partial \theta} \xi_2(\theta)^\top \frac{\partial}{\partial \theta} \mathcal{L}_{\text{ACL}}(\{x\}; \theta) \\
&\quad + \xi_1(\theta) + \sigma, \tag{8}
\end{aligned}$$

where  $\xi_1(\theta) \rightarrow 0$  and  $\xi_2(\theta) \rightarrow 0$  are the remainder terms of Taylor series. Recall that  $\mathcal{L}_{\text{RD}}(U; \theta) = \sum_{x_i \in U} \ell_{\text{RD}}(x_i; \theta)$ ,  $\mathcal{L}_{\text{ACL}}(S; \theta) = \sum_{x_i \in S} \ell_{\text{ACL}}(x_i; \theta)$ ,  $|U| = M$ , and  $|X| = N$ . According to Assumption 1, we have the following results :

$$\left\| \frac{\partial}{\partial \theta} \mathcal{L}_{\text{RD}}(U; \theta) \right\| \leq |U| L_1 = M L_1; \tag{9}$$

$$\left\| \frac{\partial^2}{\partial \theta^2} \mathcal{L}_{\text{RD}}(U; \theta) \right\| \leq |U| L_3 = M L_3; \tag{10}$$

$$\left\| \frac{\partial}{\partial \theta} \mathcal{L}_{\text{ACL}}(S; \theta) \right\| \leq |S| L_2 \leq k |X| L_2 = k N L_2; \tag{11}$$

$$\left\| \frac{\partial^2}{\partial \theta^2} \mathcal{L}_{\text{ACL}}(S; \theta) \right\| \leq |S| L_4 \leq k |X| L_4 = k N L_4. \tag{12}$$

We assume that  $\|\xi_1(\theta)\| \leq \nu_1$  and  $\|\frac{\partial}{\partial \theta} \xi_2(\theta)\| \leq \nu_2$  where  $\nu_1 \rightarrow 0^+$  and  $\nu_2 > 0$  are two positive constant. We can transform Eq. (8) as follows,

$$\begin{aligned}
\hat{G}_\theta(x|S) &\geq -\|\hat{G}_\theta(x|S)\| \\
&\geq -\eta \left\| \frac{\partial}{\partial \theta} \mathcal{L}_{\text{RD}}(U; \theta) \right\| \left\| \frac{\partial}{\partial \theta} \mathcal{L}_{\text{ACL}}(\{x\}; \theta) \right\| - \eta^2 \left\| \frac{\partial}{\partial \theta} \mathcal{L}_{\text{RD}}(U; \theta) \right\| \left\| \frac{\partial^2}{\partial \theta^2} \mathcal{L}_{\text{ACL}}(S; \theta) \right\| \left\| \frac{\partial}{\partial \theta} \mathcal{L}_{\text{ACL}}(\{x\}; \theta) \right\| \\
&\quad - \eta^2 \left\| \frac{\partial}{\partial \theta} \mathcal{L}_{\text{ACL}}(S; \theta) \right\| \left\| \frac{\partial^2}{\partial \theta^2} \mathcal{L}_{\text{RD}}(U; \theta) \right\| \left\| \frac{\partial}{\partial \theta} \mathcal{L}_{\text{ACL}}(\{e\}; \theta) \right\| - \left\| \frac{\partial}{\partial \theta} \xi_2(\theta) \right\| \left\| \frac{\partial}{\partial \theta} \mathcal{L}_{\text{ACL}}(\{x\}; \theta) \right\| \\
&\quad - \|\xi_1(\theta)\| + \sigma \\
&\geq -\eta M L_1 L_2 - \eta^2 M L_1 k N L_4 L_2 - \eta^2 k N L_2 M L_3 L_2 - \nu_2 L_2 - \nu_1 + \sigma \\
&\geq -\eta M L_2(L_1 + \eta k N(L_1 L_4 + L_2 L_3)) - \nu_2 L_2 - \nu_1 + \sigma.
\end{aligned}$$

Since  $\sigma = \eta M L_2(L_1 + \eta k N(L_1 L_4 + L_2 L_3)) + \nu_1 + \nu_2 L_2 + 1$ , we can obtain that

$$\hat{G}_\theta(x|S) \geq 1. \tag{13}$$

Eq. (13) shows that  $\hat{G}_\theta(S)$  is monotone, i.e.,  $\hat{G}_\theta(x|S) > 0$ .

Then, we provide **proof of  $\gamma$ -weakly submodularity of  $\hat{G}_\theta(S)$** . The sketch of proof is that we first prove  $\hat{G}_\theta(S)$  is  $\alpha$ -submodular. Then, according to Lemma 1, we can conclude that  $\hat{G}_\theta(S)$  is also  $\gamma$ -weakly submodular.

**Lemma 1** (Proposition 4 of Gatmiry and Gomez-Rodriguez (2021)). *The set function  $G(S) : 2^X \rightarrow \mathbb{R}$  that is  $\alpha$ -submodular is  $\gamma$ -weakly submodular with the submodularity ratio  $\gamma \geq 1 - \alpha$ .*

The following is the definition of  $\alpha$ -submodularity.

**Definition 2** ( $\alpha$ -submodularity (Gatmiry and Gomez-Rodriguez, 2021)). *A function is called  $\alpha$ -submodular if the marginal gain of adding an element  $x$  to set  $A$  is  $1 - \alpha$  times greater than or equals to the gain of adding an element  $x$  to set  $B$  where  $A \subseteq B$ . i.e.,*

$$\forall_{A, B | A \subseteq B} G_\theta(x|A) \geq (1 - \alpha)G_\theta(x|B).$$

According to Eq. (13), we have obtained the lower bound of the marginal gain

$$\hat{G}_\theta(x|S) \geq 1 = \underline{\hat{G}}_\theta(S). \quad (14)$$

We can obtain the upper bound of marginal gain based on Eq. (8) as follows,

$$\begin{aligned} \hat{G}_\theta(x|S) &\leq \eta \left\| \frac{\partial}{\partial \theta} \mathcal{L}_{\text{RD}}(U; \theta) \right\| \left\| \frac{\partial}{\partial \theta} \mathcal{L}_{\text{ACL}}(\{x\}; \theta) \right\| + \eta^2 \left\| \frac{\partial}{\partial \theta} \mathcal{L}_{\text{RD}}(U; \theta) \right\| \left\| \frac{\partial^2}{\partial \theta} \mathcal{L}_{\text{ACL}}(S; \theta) \right\| \left\| \frac{\partial}{\partial \theta} \mathcal{L}_{\text{ACL}}(\{x\}; \theta) \right\| \\ &\quad + \eta^2 \left\| \frac{\partial}{\partial \theta} \mathcal{L}_{\text{ACL}}(S; \theta) \right\| \left\| \frac{\partial^2}{\partial \theta} \mathcal{L}_{\text{RD}}(U; \theta) \right\| \left\| \frac{\partial}{\partial \theta} \mathcal{L}_{\text{ACL}}(\{x\}; \theta) \right\| + \left\| \frac{\partial}{\partial \theta} \xi_2(\theta) \right\| \left\| \frac{\partial}{\partial \theta} \mathcal{L}_{\text{ACL}}(\{x\}; \theta) \right\| \\ &\quad + \|\xi_1(\theta)\| + \sigma \\ &\leq \eta M L_1 L_2 + \eta^2 M L_1 k N L_4 L_2 + \eta^2 k N L_2 M L_3 L_2 + \nu_2 L_2 + \nu_1 + \sigma \\ &\leq \eta M L_2 (L_1 + \eta k N (L_1 L_4 + L_2 L_3)) + \nu_2 L_2 + \nu_1 + \sigma. \end{aligned}$$

Since  $\sigma = \eta M L_2 (L_1 + \eta k N (L_1 L_4 + L_2 L_3)) + \nu_2 L_2 + \nu_1 + 1$ , we can obtain that

$$\hat{G}_\theta(x|S) \leq 2\eta M L_2 (L_1 + \eta k N (L_1 L_4 + L_2 L_3)) + 2\nu_1 + 2\nu_2 L_2 + 1 = 2\sigma - 1 = \overline{\hat{G}}_\theta(S). \quad (15)$$

Based on the lower bound (Eq. (14)) and the upper bound (Eq. (15)) of the marginal gain function, we can obtain

$$\frac{\hat{G}_\theta(x|A)}{\hat{G}_\theta(x|B)} \geq \frac{\underline{\hat{G}}_\theta(S)}{\overline{\hat{G}}_\theta(S)} = \frac{1}{2\eta M L_2 (L_1 + \eta k N (L_1 L_4 + L_2 L_3)) + 2\nu_1 + 2\nu_2 L_2 + 1} = \frac{1}{2\sigma - 1} = 1 - \alpha^* \in (0, 1). \quad (16)$$

Therefore, we have proved  $\hat{G}_\theta(S)$  is  $\alpha^*$ -submodular. According to Lemma 1,  $\hat{G}_\theta(S)$  is  $\gamma$ -weakly submodular where  $\gamma > \gamma^* = \frac{1}{2\sigma - 1}$ . □

## A.2 Proof of Theorem 2

**Theorem 2 (Restated)** *Given a fixed parameter  $\theta$ , we denote the optimal solution of Eq. (6) as  $G_\theta^* = \sup_{S \subseteq X, |S|/|X|=k} G_\theta(S)$ . Then,  $\hat{S}^*$  in Eq. (7) found via greedy search satisfies*

$$G_\theta(\hat{S}^*) \geq G_\theta^* - (G_\theta^* + kN\sigma) \cdot e^{-\gamma^*}.$$

*Proof.* We provide the lemma that describes the optimality guarantee of the greedy search algorithm in the problem of maximizing a monotone  $\alpha$ -approximate submodular function subject to cardinality constraints.

**Lemma 2** ((Das and Kempe, 2011; Gatmiry and Gomez-Rodriguez, 2021)). *Given a monotone and  $\alpha$ -approximate submodular function  $G(S)$ , the greedy search algorithm achieves a  $1 - e^{-(1-\alpha)}$  approximation factor for the problem of maximizing  $G(S)$  subject to cardinality constraints.*

Note that according to Theorem 1,  $\hat{G}_\theta(S)$  is a monotone and  $\alpha^*$ -approximate submodular function. Therefore, according to Lemma 2, we have

$$\hat{G}_\theta(\hat{S}^*) \geq (1 - e^{-\gamma^*})\hat{G}_\theta^*, \quad (17)$$

where  $\hat{G}_\theta^* = \sup_{S \subseteq X, |S|/|X|=k} \hat{G}_\theta(S)$  and  $\hat{S}^*$  is found via greedy search. Since  $\hat{G}_\theta(S) = G_\theta(S) + |S|\sigma$ , we have

$$\hat{G}_\theta^* = \sup_{S \subseteq X, |S|/|X|=k} (G_\theta(S) + |S|\sigma) = \sup_{S \subseteq X, |S|/|X|=k} G_\theta(S) + k|X|\sigma = G_\theta^* + kN\sigma. \quad (18)$$

Recall that  $\hat{G}_\theta(\hat{S}^*) = G_\theta(\hat{S}^*) + kN\sigma$ . Therefore, by transforming Eq. (17), we can obtain

$$G_\theta(\hat{S}^*) \geq G_\theta^* - (G_\theta^* + kN\sigma) \cdot e^{-\gamma^*}. \quad (19)$$

□

## B Extensive Experimental Details and Results

### B.1 An Extra Trick to Enable Efficient RCS on Large-Scale Datasets with Limited GPU Memory

RCS on large-scale datasets such as ImageNet-1K (Deng et al., 2009) needs to calculate the loss gradient for each minibatch of training data as the first step (Line 5–7 in Algorithm 1). Then, the greedy search is conducted to iteratively select the minibatch that has the largest marginal gain and add this minibatch into the final coreset (Line 9–19 in Algorithm 1). Saving the gradients of all the minibatches on GPU needs a large amount of GPU memory. When the GPU memory is limited, there exists an issue that we are unable to save all the gradients on GPU.

A direct solution is to transfer the loss gradients from GPU to CPU and save all the gradients on CPU. When we need to use the loss gradient of a minibatch, we can transfer the gradient from CPU to GPU for calculation. Unexpectedly, the transition between CPU and GPU still consumes a large amount of time in practice. Thus, we do not take this solution.

To solve this issue, we split the entire training set into several training subsets. Practically, we take every 100 minibatches of training data as a training subset. Then, we conduct RCS on each training subset respectively and collect the coresets from each training subset together as the final coresets for robust pre-training. In this way, we can enable RCS to efficiently search for the coresets from large-scale datasets with limited GPU memory. We apply this trick to the experiments regarding ACL on ImageNet-1K in Section 4.3 and SAT on ImageNet-1K in Section 4.2.

### B.2 Complementary Experimental Details

We conducted all experiments on Python 3.8.8 (PyTorch 1.13) with 4 NVIDIA RTX A5000 GPUs (CUDA 11.6).

**Using the dual Batch Normalization (BN) for ACL** Following Jiang et al. (2020), we leveraged the dual BN (Xie et al., 2020), where one BN is used for the standard branch of the feature extractor and the other BN is used for the adversarial branch, during conducting ACL on CIFAR-10 (details in Section 4.1) and ImageNet-1K (details in Section 4.3).

**Experimental details of standard finetuning.** To evaluate the standard transferability of pre-trained ResNet-18 models via ACL on CIFAR-10, we standardly trained the pre-trained models on the downstream tasks (i.e., CIFAR-100 and SVHN (Netzer et al., 2011)), for 100 epochs using SGD with an initial learning rate 0.1 divided by 10 at epoch 40 and 60. The learning objective of standard training is  $\mathcal{L}_{\text{Standard}}(\cdot)$  shown in Section 2.2.

To evaluate the standard transferability of pre-trained WRN-28-10 models via ACL on ImageNet-1K of  $32 \times 32$  resolution, we standardly trained the pre-trained WRN-28-10 models on CIFAR-10 and CIFAR-100 for 150 epochs using SGD. We set the initial learning rate as 0.1 for standard full finetuning and 0.01 for standard partial finetuning. The learning rate is divided by 10 at epoch 50 and 100.

**Experimental details of robustness finetuning.** To evaluate the robustness transferability of pre-trained ResNet-18 models via ACL on CIFAR-10, we adversarially trained the pre-trained ResNet-18 models on SVHN and CIFAR-100 for 100 epochs using SGD with an initial learning rate 0.1 divided by 10 at epoch 40 and 60. Adversarial training data during robust finetuning is generated via PGD with 10 PGD steps, adversarial budget  $8/255$ , and step size  $2/255$ . Here, we followed Jiang et al. (2020) using TRADES (Zhang et al., 2019) whose learning objective is  $\mathcal{L}_{\text{TRADES}}(\cdot)$  in Eq. (21) for robust finetuning.



Table 3: We show the test accuracy of standardly pre-trained ResNet-18 on downstream tasks (i.e., SVHN and CIFAR-100) for checking the absolute test accuracy in Figure 2, 6, and 7. The standardly pre-trained ResNet-18 is pre-trained via Standard CL (Chen et al., 2020) on CIFAR-10 without using labels.

Downstream tasks	Standard test accuracy		Robust test accuracy	
	Standard full finetuning	Standard partial finetuning	Robust full finetuning	Robust partial finetuning
SVHN	95.25%	45.72%	48.01%	1.53%
CIFAR-100	77.66%	36.28%	23.51%	0.00%

Table 4: We show the test accuracy of standardly pre-trained ResNet-18 on downstream tasks (i.e., CIFAR-100) for checking the absolute test accuracy in Figure 10. The standardly pre-trained ResNet-18 is pre-trained via standard training on CIFAR-10 using labels.

Downstream tasks	Standard test accuracy		Robust test accuracy	
	Standard full finetuning	Standard partial finetuning	Robust full finetuning	Robust partial finetuning
CIFAR-100	77.43%	22.93%	27.57%	0.01%

Table 5: We show the test accuracy of standardly pre-trained WRN-28-10 on downstream tasks (i.e., CIFAR-10 and CIFAR-100) for checking the absolute test accuracy in the upper panels of Figure 4. The standardly pre-trained WRN-28-10 is standardly pre-trained on ImageNet-1K of  $32 \times 32$  resolution using labels.

Downstream tasks	Robust test accuracy	
	Robust full finetuning	Robust partial finetuning
CIFAR-10	51.91%	10.00%
CIFAR-100	27.81%	0.00%

Table 6: We show the test accuracy of standardly pre-trained ResNet-50 on downstream tasks (i.e., CIFAR-10 and CIFAR-100) for checking the absolute test accuracy in the lower panels of Figure 4. The standardly pre-trained ResNet-50 on ImageNet-1K is downloaded from PyTorch.

Downstream tasks	Standard test accuracy	
	Standard full finetuning	Standard partial finetuning
CIFAR-10	97.34%	74.57%
CIFAR-100	84.85%	46.47%

To evaluate the robustness transferability of pre-trained WRN-28-10 models via ACL on ImageNet-1K of  $32 \times 32$  resolution, we adversarially trained the pre-trained WRN-28-10 models on CIFAR-10 and CIFAR-100 for 30 epochs using SGD. We set the initial learning rate as 0.1 for robust full finetuning and 0.01 for robust partial finetuning. The learning rate is divided by 10 at epoch 10 and 20. The learning objective of robust finetuning exactly follows  $\mathcal{L}_{\text{Robust}}(\cdot)$  shown in Section 2.2.

**How can we obtain standardly pre-trained models on the entire set?** To obtain models pre-trained via standard CL, we leveraged SimCLR (Chen et al., 2020) as the standard CL to pre-train ResNet-18 models on CIFAR-10 following the settings in Section 4.1 and WRN-28-10 models on ImageNet-1K of  $32 \times 32$  resolution following the settings in Section 4.3.

To obtain models pre-trained via standard training, we standardly pre-train ResNet-18 and WRN-28-10 on ImageNet-1K of  $32 \times 32$  resolution. The training settings follow those of SAT in Section 4.2. As for ResNet-50 standardly pre-trained on ImageNet-1K of  $224 \times 224$  resolution, we use the pre-trained ResNet-50 ( $\epsilon = 0$ ) published in this GitHub (Salman et al., 2020).

Tables 3–6 show the test accuracy achieved by standardly pre-trained models on downstream tasks. The absolute test accuracy of the adversarially pre-trained model is the sum of the test accuracy achieved by the standardly pre-trained model and the relative accuracy achieved by the adversarially pre-trained models on the downstream task.

**How can we obtain adversairally pre-trained models on the entire set?** We pre-trained ResNet-18 on the entire training set of CIFAR-10 via ACL following the training settings of ACL (Jiang et al., 2020).

Due to the extremely long pre-training time of ACL on the entire set (as shown in Table 7), we do not provide the results of ACL on the full set of ImageNet-1K. We only provide the results of ACL on the coreset in Table 1 and 2.

As for pre-trained models via SAT on the entire set of ImageNet-1K, we use WRN-28-10 pre-trained on ImageNet-1K of  $32 \times 32$  resolution provided by Hendrycks et al. (2019) and ResNet-50 ( $\epsilon = 4.0$ ) pre-trained on ImageNet-1K of  $224 \times 224$  resolution provided by Salman et al. (2020).

Table 7 demonstrates the approximated training time on the entire set of various models via ACL (Jiang et al., 2020), SAT (Madry et al., 2018), and TRADES (Zhang et al., 2019), respectively. All the running time was evaluated

Table 7: Running time (hours) on the entire training set of various models via ACL, SAT, and TRADES.

Pre-training on the entire set	ResNet-18 on CIFAR-10	ResNet-50 on ImageNet-1K	WRN-28-10 on ImageNet-1K
ACL (Jiang et al., 2020)	38.9	-	650.2
SAT (Madry et al., 2018)	5.2	286.1	341.7
TRADES (Zhang et al., 2019)	5.5	-	-

Table 8: We show the robust test accuracy evaluated by AutoAttack (AA) (Croce and Hein, 2020) of standardly pre-trained ResNet-18 on downstream tasks (i.e., SVHN and CIFAR-100) for checking the absolute robust test accuracy in Figure 5. The standardly pre-trained ResNet-18 is standardly pre-trained on CIFAR-10 without using labels.

Downstream tasks	Robust test accuracy (AA)	
	Robust full finetuning	Robust partial finetuning
SVHN	41.38%	1.53%
CIFAR-100	19.71%	0.00%

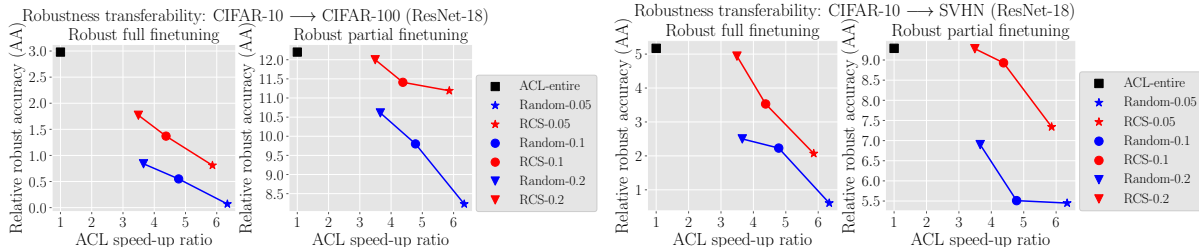


Figure 5: Robustness transferability evaluated by AutoAttack (AA) (Croce and Hein, 2020) from CIFAR-10 to CIFAR-100 and SVHN of ACL pre-trained ResNet-18 with various CS strategies. “ACL-entire” denotes ACL on the entire training set of CIFAR-10. The number after the dash line denotes the subset fraction  $k \in \{0.05, 0.1, 0.2\}$ .

on NVIDIA RTX A5000 GPUs. We used 1 GPU for pre-training on ResNet-18 and 4 GPUs for pre-training on ImageNet-1K.

### B.3 Experimental Details of Figure 1

In Figure 1, we report the transferability of pre-trained ResNet-18 from CIFAR-10 to CIFAR-100. ACL with RCS and ACL with random selection use the subset fraction  $k = 0.05$  and  $\omega = 100$ . Other pre-training settings of ACL on CIFAR-10 exactly keep the same as Section 4.1. In Figure 1, we show the robustness transferability of pre-trained ResNet-18 after the procedure of robust partial finetuning on CIFAR-100, and the standard transferability of pre-trained ResNet-18 after the procedure of standard full finetuning on CIFAR-100.

### B.4 Robustness Transferability Evaluated by AutoAttack

In this section, we evaluate robust accuracy by AutoAttack (AA) (Croce and Hein, 2020) to empirically validate that the robustness gain achieved by ACL with RCS is not due to the gradient obfuscation (Athalye et al., 2018). Figure 5 demonstrates the robustness transferability from CIFAR-10 to CIFAR-100 and SVHN of pre-trained ResNet-18 via ACL with RCS. Training settings exactly follow Section 4.1. Table 8 shows the robust test accuracy evaluated by AA of standardly pre-trained ResNet-18 for checking the absolute robust test accuracy. It shows that ACL with RCS always performs better robustness transferability compared with ACL with Random under the evaluation of AA. Besides, ACL with RCS consistently achieves better robust accuracy evaluated by AA on downstream tasks compared with Standard CL since the value of the red line is always above 0. Therefore, it validates that ACL with RCS indeed provides pre-trained models with better robustness transferability compared with Standard CL.

### B.5 Efficient ACL via RCS with Various Distance Functions $\Phi$

This section provides the results of ACL with RCS using different distance functions including the KL divergence (Zhang et al., 2019), the JS divergence (Addepalli et al., 2022), and the OT distance (Zhang and Wang, 2019) for calculating the RD  $\mathcal{L}_{RD}(\cdot)$ . Other training settings exactly keep the same as Section 4.1. Figure 6 shows that efficient ACL via RCS with various distance functions can consistently obtain better transferability compared with Random. Especially, RCS with KL divergence often achieves better transferability to downstream tasks among different distance functions. Therefore, we use KL divergence for RCS in all the experiments in the main paper.

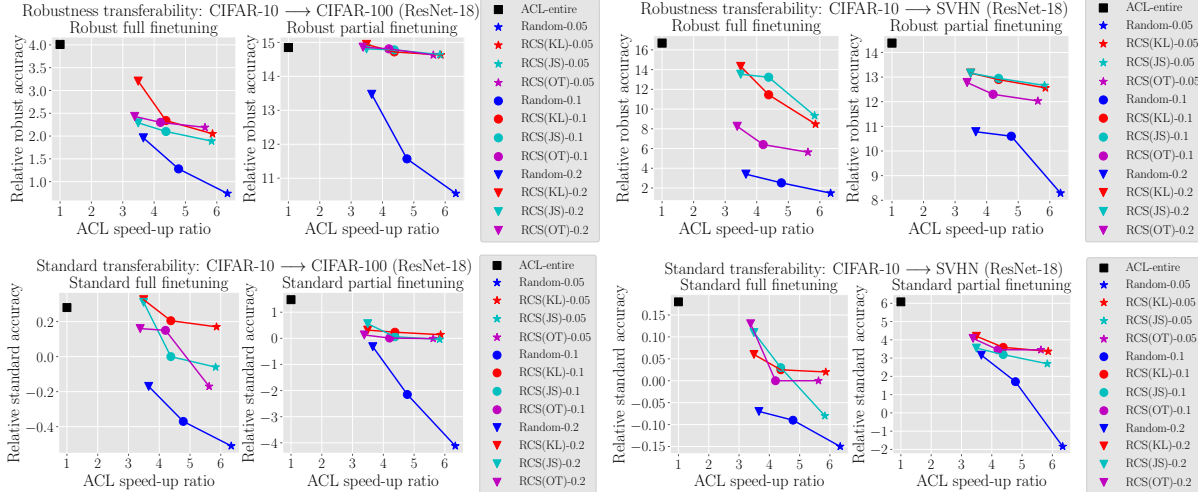


Figure 6: Robustness transferability (upper panels) and standard transferability (lower panels) from CIFAR-10 to CIFAR-100 and SVHN of ACL pre-trained ResNet-18 with various distance functions (denoted in parentheses). “ACL-entire” denotes ACL on the entire training set of CIFAR-10. The number after the dash line denotes the subset fraction  $k \in \{0.05, 0.1, 0.2\}$ .

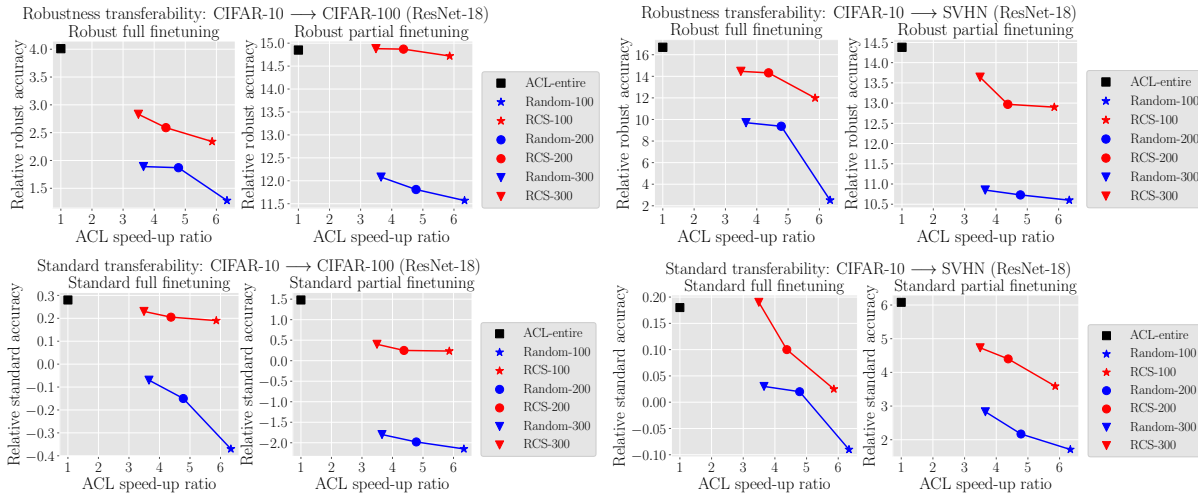


Figure 7: Robustness transferability (upper panels) and standard transferability (lower panels) from CIFAR-10 to CIFAR-100 and SVHN of ACL pre-trained ResNet-18 with various warmup epochs. “ACL-entire” denotes ACL on the entire training set of CIFAR-10. The number after the dash line denotes the warmup epoch  $\omega \in \{100, 200, 300\}$ .

## B.6 Efficient ACL via RCS with Various Warmup Epochs $\omega$

This section provides the results of RCS with different warmup epochs  $\omega \in \{100, 200, 300\}$  for efficient ACL. We set the subset fraction  $k$  as 0.1. Other training settings follow Section 4.1. Figure 7 shows that as the warmup epoch of RCS (red lines) increases, the transferability becomes better. Meanwhile, ACL with RCS consistently achieves better transferability compared with ACL with Random, which validates the effectiveness of RCS in efficient ACL.

## B.7 RCS for Accelerating a Variant of ACL Method

Fan et al. (2021) proposed a variant of ACL method, called “AdvCL”, that leverages a standardly pre-trained model on ImageNet-1K to generate pseudo-labels for CIFAR-10 training data via  $K$ -means clustering. Based on ACL (Jiang et al., 2020), the loss function of AdvCL is composed of a weighted sum of the adversarial contrastive loss and an ensemble of the CE loss between the adversarial data and its pseudo label over different choices of cluster number. By simply replacing the loss function of the ACL  $\mathcal{L}_{\text{ACL}}(\cdot)$  with that of AdvCL in Algorithm 1 and 2, we can apply RCS for efficient AdvCL.

Table 9: The transferability from CIFAR-10 to CIFAR-100 of pre-trained ResNet-18 models via standard CL (Chen et al., 2020), ACL (Jiang et al., 2020), and AdvCL (Fan et al., 2021). As for the configuration of the coreset selection, we set warmup epoch  $\omega = 100$ , the subset fraction  $k = 0.1$ , and the epoch interval  $\lambda = 20$  for conducting RCS.

Pre-training	Runing time (hours)	Standard test accuracy		Robust test accuracy	
		Standard full finetuning	Standard partial finetuning	Robust full finetuning	Robust partial finetuning
Standard CL	7.8	77.66%	36.28%	23.51%	0.00%
ACL on entire set	38.9	77.94%	37.76%	27.53%	14.84%
ACL with Random	8.1	77.29%	34.16%	24.79%	11.57%
ACL with RCS	10.7	77.87%	36.52%	25.74%	14.75%
AdvCL on entire set	57.8	77.73%	15.81%	30.84%	1.54%
AdvCL with Random	11.0	76.97%	14.81%	29.81%	1.05%
AdvCL with RCS	13.5	77.71%	15.65%	30.54%	1.52%

We pre-trained ResNet-18 via AdvCL with RCS on CIFAR-10 using SGD for 1000 epochs with an initial learning rate 0.5 and a cosine annealing scheduler. We set  $\beta = 512$ ,  $T_{\text{ACL}} = 5$ ,  $\epsilon_{\text{ACL}} = 8/255$ ,  $\rho_{\text{ACL}} = 2/255$ , and  $T_{\text{RCS}} = 3$ . The training settings of AdvCL exactly follow Fan et al. (2021). We take the same configuration of RCS as that of RCS for ACL in Section 4.1, i.e., warmup epoch  $\omega = 100$ , the epoch interval for conducting RCS  $\lambda = 20$ , and the subset fraction  $k = 0.1$ . Then, we finetuned the pre-trained ResNet-18 models on CIFAR-100 and the settings of finetuning procedure exactly follow Section 4.1. We demonstrate the transferability from CIFAR-10 to CIFAR-100 of pre-trained ResNet-18 models in Table 9.

Table 9 shows that RCS can indeed speed up AdvCL (Fan et al., 2021). Besides, RCS is a principled method that helps AdvCL to obtain effective robust representations since AdvCL with RCS always achieves a higher test accuracy compared with AdvCL with Random. Meanwhile, we can observe that RCS can almost maintain transferability since the performance of AdvCL with RCS is slightly worse than AdvCL on the entire set. In addition, we can find that AdvCL always achieves a lower test accuracy after partial finetuning compared with ACL (Jiang et al., 2020), which empirically shows that ACL is an effective unsupervised robust pre-training method. Notably, our proposed RCS can speed up both ACL and AdvCL without largely sacrificing the transferability of the pre-trained models. Therefore, the experimental results validate that our proposed RCS can be a unified and effective framework for accelerating ACL as well as its variants.

## B.8 Extensive Visualization of Feature Representations

Here, we demonstrate extra visualization of feature representations of ACL pre-trained ResNet-18 using t-SNE (Van der Maaten and Hinton, 2008). Figure 8 demonstrates RCS can help the model obtain a good feature representation with a more clear decision boundary compared with Random. It validates the effectiveness of RCS in speeding up ACL while obtaining useful representations.

## B.9 RCS for Accelerating Supervised AT

In this section, we first provide the algorithm of RCS for supervised AT, i.e., standard adversarial training (SAT) (Madry et al., 2018) and TRADES (Zhang et al., 2019). Then, we show the results of SAT and TRADES with RCS on CIFAR-10 and the experimental details of SAT with RCS on ImageNet-1K.

**Algorithm of RCS for supervised AT.** Prior to introducing the algorithm of RCS for SAT and TRADES, we first provide the preliminaries of SAT and TRADES.

Given a labeled training set  $D = \{(x_i, y_i)\}_{i=1}^N$ , where data  $x_i \in \mathcal{X}$  and label  $y_i \in \mathcal{Y} = \{0, 1, \dots, C - 1\}$ , a feature extractor  $f_\theta : \mathcal{X} \rightarrow \mathcal{Z}$ , a randomly initialized classifier  $g : \mathcal{Z} \rightarrow \mathbb{R}^C$ , the loss function of SAT is

$$\mathcal{L}_{\text{SAT}}(D; \theta) = \sum_{i=1}^N \left\{ \max_{\tilde{x}_i \in \mathcal{B}_\epsilon[x_i]} \ell(g \circ f_\theta(\tilde{x}_i), y_i) \right\}, \quad (20)$$

where  $\ell$  is the Cross-Entropy (CE) loss and  $\tilde{x}_i$  is adversarial training data generated by PGD within the  $\epsilon$ -ball centered at  $x_i$ .

The loss function of TRADES is

$$\mathcal{L}_{\text{TRADES}}(D; \theta) = \sum_{i=1}^N \left\{ \ell(g \circ f_\theta(x_i), y_i) + c \cdot \max_{\tilde{x}_i \in \mathcal{B}_\epsilon[x_i]} KL(g \circ f_\theta(\tilde{x}_i), g \circ f_\theta(x_i)) \right\}, \quad (21)$$

where  $\ell$  is the CE loss,  $KL(\cdot, \cdot)$  is the KL divergence,  $c > 0$  is a trade-off parameter, and  $\tilde{x}_i$  is adversarial training data generated by PGD within the  $\epsilon$ -ball centered at  $x_i$ . We set  $c = 6$ , following Zhang et al. (2019). Note that the

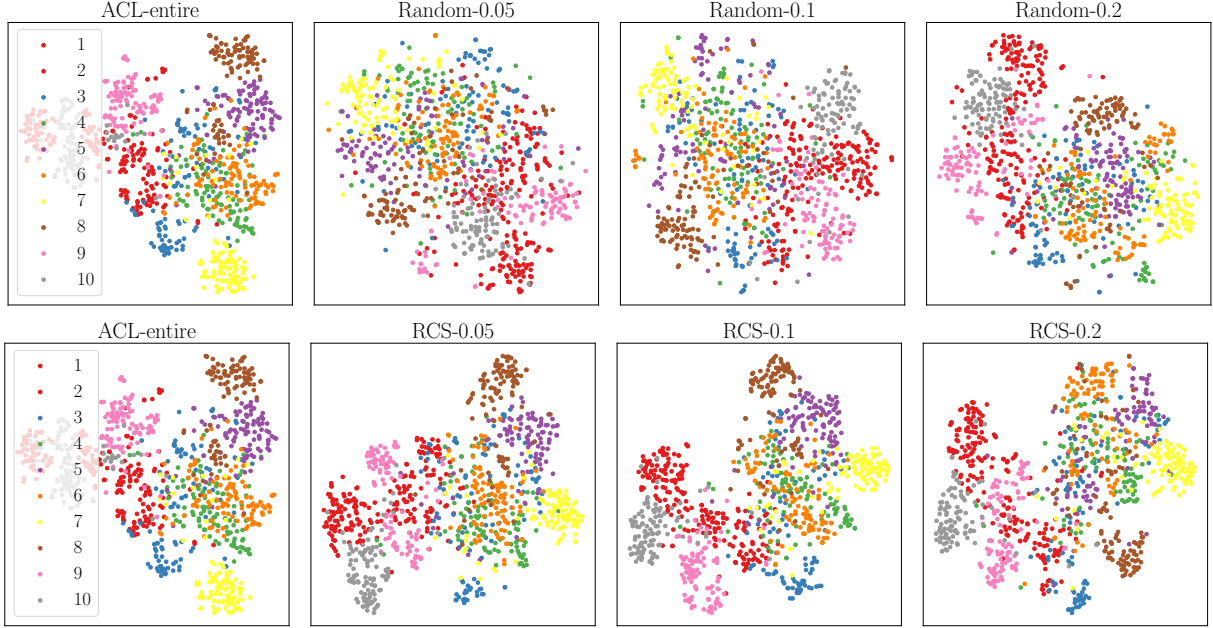


Figure 8: Feature representations generated by ACL pre-trained models. “ACL-entire” denotes ACL on the entire training set of CIFAR-10. The number after dash line denotes the subset fraction  $k \in \{0.1, 0.2, 0.3\}$ .

parameters of  $g$  are updated during supervised AT. Here we omit the parameters of  $g$  since we only use the parameters of the feature extractor  $f_\theta$  in downstream tasks.

The RCS problem for supervised AT is formulated as follows:

$$S^* = \arg \max_{S \subseteq D, |S|/|D|=k} -\mathcal{L}_{RD}(U; \theta - \eta \nabla_\theta \mathcal{L}_{supervised}(S; \theta)), \quad (22)$$

in which we replace the ACL loss  $\mathcal{L}_{ACL}(\cdot)$  in Eq. (6) with the supervised AT loss  $\mathcal{L}_{supervised}(\cdot)$  (e.g.,  $\mathcal{L}_{SAT}(\cdot)$  and  $\mathcal{L}_{TRADES}(\cdot)$ ). Due to that  $\mathcal{L}_{RD}(\cdot)$  only needs data and does not need any label, RCS is applicable to supervised AT, no matter if the validation set is unlabeled or labeled. By leveraging greedy search, we show the algorithm of RCS for supervised AT in Algorithm 3 and efficient supervised AT via RCS in Algorithm 4.

**Efficient supervised AT via RCS on CIFAR-10.** We pre-trained ResNet-18 on CIFAR-10 via SAT using SGD with 0.9 momentum for 120 epochs with the initial learning rate of 0.1 divided by 10 at epoch 30 and 60. For PGD configurations during SAT, we set  $\beta = 128$ ,  $T_{SAT} = 10$ ,  $\epsilon_{SAT} = 8/255$ ,  $\rho_{SAT} = 2/255$ . During RCS, we set  $T_{RCS} = 3$ . We took  $\omega = 30$  epochs for warmup, and then CS was conducted every  $\lambda = 10$  epochs. We adversarially pre-trained ResNet-18 with different subset fractions  $k \in \{0.05, 0.1, 0.2\}$  and then conducted robust finetuning on CIFAR-100. The results are shown in the left panel of Figure 9 and the upper panels of Figure 10.

We pre-trained ResNet-18 on CIFAR-10 via TRADES using SGD with 0.9 momentum for 100 epochs with the initial learning rate of 0.1 divided by 10 at epoch 60 and 90. For PGD configurations during TRADES, we set  $T_{TRADES} = 10$ ,  $\epsilon_{TRADES} = 8/255$ ,  $\rho_{TRADES} = 2/255$ . Other training settings follow SAT. The results of TRADES pre-trained models are shown in the right panel of Figure 9 and the lower panels of Figure 10.

To evaluate the robustness transferability of pre-trained ResNet-18 models via supervised AT on CIFAR-10, we adversarially finetuned the pre-trained models on CIFAR-100 for 100 epochs using SGD with an initial learning rate 0.1 divided by 10 at epoch 40 and 60. The learning objective of robust finetuning exactly follows  $\mathcal{L}_{Robust}(\cdot)$  shown in Section 2.2.

To evaluate the standard transferability of pre-trained ResNet-18 models via supervised AT on CIFAR-10, we standardly finetuned the pre-trained models on CIFAR-100 for 100 epochs using SGD with an initial learning rate 0.1 divided by 10 at epoch 40 and 60. The learning objective of standard training is  $\mathcal{L}_{Standard}(\cdot)$  shown in Section 2.2.

Here, we used ACS (Dolatabadi et al., 2022) and random selection (dubbed as “Random”) as the baseline. The implementation of ACS exactly follows the public GitHub of ACS (Dolatabadi et al., 2022). We use the same subset fraction and warmup epoch for both ACS and random selection as RCS.

---

**Algorithm 3** RCS for supervised AT

---

- 1: **Input:** Labeled training set  $D$ , validation set  $U$ , batch size  $\beta$ , model  $g \circ f_\theta$ , learning rate for RCS  $\eta$ , subset fraction  $k \in (0, 1]$ , loss function of supervised AT method  $\mathcal{L}_{supervised}(\cdot)$
- 2: **Output:** Coreset  $S$
- 3: Initialize  $S \leftarrow \emptyset$
- 4: Split entire set into minibatches  $D = \{B_m\}_{m=1}^{\lceil |D|/\beta \rceil}$
- 5: **for** each minibatch  $B_m \in D$  **do**
- 6:   Compute gradient  $q_m \leftarrow \nabla_\theta \mathcal{L}_{supervised}(B_m; \theta)$
- 7: **end for**
- 8: // Conduct greedy search via batch-wise selection
- 9: **for**  $1, \dots, \lfloor k|D|/\beta \rfloor$  **do**
- 10:   Compute gradient  $q_U \leftarrow \nabla_\theta \mathcal{L}_{RD}(U; \theta)$
- 11:   Initialize  $best\_gain = -\infty$
- 12:   **for** each minibatch  $B_m \in D$  **do**
- 13:     Compute marginal gain  $\hat{G}(B_m|S) \leftarrow \eta q_U^\top q_m$
- 14:     **if**  $\hat{G}(B_m|S) > best\_gain$  **then**
- 15:       Update  $s \leftarrow m, best\_gain \leftarrow \hat{G}(B_m|S)$
- 16:     **end if**
- 17:   **end for**
- 18:   Update  $S \leftarrow S \cup B_s, D \leftarrow D \setminus B_s$
- 19:   Update  $\theta \leftarrow \theta - \eta q_s$
- 20: **end for**

---

---

**Algorithm 4** Efficient supervised AT via RCS

---

- 1: **Input:** Labeled training set  $D$ , validation set  $U$ , total training epochs  $E$ , learning rate  $\eta'$ , batch size  $\beta$ , warmup epoch  $\omega$ , epoch interval for executing RCS  $\lambda$ , subset fraction  $k$ , learning rate for RCS  $\eta$ , loss function of supervised AT method  $\mathcal{L}_{supervised}(\cdot)$
- 2: **Output:** robust pre-trained feature extractor  $f_\theta$
- 3: Initialize parameters of model  $g \circ f_\theta$
- 4: Initialize training set  $S \leftarrow D$
- 5: **for**  $e = 1$  **to**  $E$  **do**
- 6:   **if**  $e\% \lambda == 0$  **and**  $e \geq \omega$  **then**
- 7:      $S \leftarrow \text{RCS}(D, U, \beta, g \circ f_\theta, \eta, k, \mathcal{L}_{supervised}(\cdot))$  //by Algorithm 3
- 8:   **end if**
- 9:   **for** batch  $m = 1, \dots, \lceil |S|/\beta \rceil$  **do**
- 10:     Sample a minibatch  $B_m$  from  $S$
- 11:     Update  $\theta \leftarrow \theta - \eta' \mathcal{L}_{supervised}(B_m; \theta)$
- 12:   **end for**
- 13: **end for**

---

In Figure 9, we use the robust test accuracy of adversarial data generated via PGD-20 to evaluate adversarial robustness. It shows that red lines are always located at the right upper corner, which indicates ACL with RCS achieves better adversarial robustness of pre-trained models with a higher speed-up ratio compared with ACL with Random (blue lines). Besides, ACL with RCS achieves similar robust test accuracy to ACL with ACS, which indicates the effectiveness of our proposed RCS in preserving the adversarial robustness of pre-trained models and thus attaining robust representations.

Figure 10 demonstrates that efficient supervised AT via RCS (red lines) consistently performs better transferability compared with efficient supervised AT with Random (blue lines). Besides, we can find that RCS gains a higher speed-up ratio than ACS (green lines), which indicates that RCS via greedy search spends less time searching for the coreset than ACS. Meanwhile, ACL with RCS always achieves higher robust and standard test accuracy on the downstream tasks than ACL with ACS. It validates that RCS is an effective method for efficient supervised AT to obtain robust representations with minor degradation in transferability.

**Experimental details of efficient SAT via RCS on ImageNet-1K.** Following Hendrycks et al. (2019), we pre-trained WRN-28-10 on ImageNet-1K of  $32 \times 32$  resolution using SAT (Madry et al., 2018). The model was trained using SGD with 0.9 momentum for 100 epochs with an initial learning rate of 0.1 and a cosine decay scheduler. For PGD configurations during SAT, we set  $\beta = 256, T_{\text{SAT}} = 10, \epsilon_{\text{SAT}} = 8/255, \rho_{\text{SAT}} = 2/255$ . We set  $T_{\text{RCS}} = 3$  during RCS. We took  $\omega = 10$  epochs for warmup, and then CS was executed every  $\lambda = 10$  epochs. We adversarially pre-train



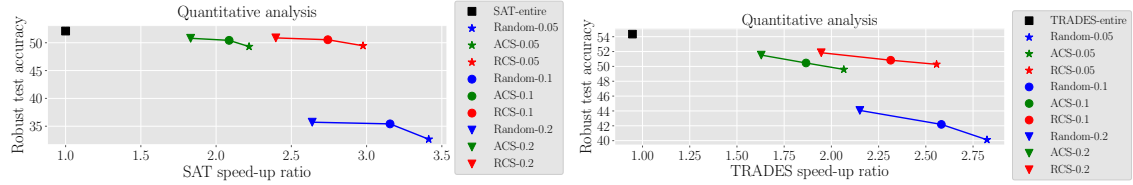


Figure 9: Adversarial robustness of SAT (left panel) and TRADES (right panel) pre-trained ResNet-18 evaluated on CIFAR-10. “entire” denotes supervised AT on the entire training set of CIFAR-10. The number after the dash line denotes the subset fraction  $k \in \{0.1, 0.2, 0.3\}$ .

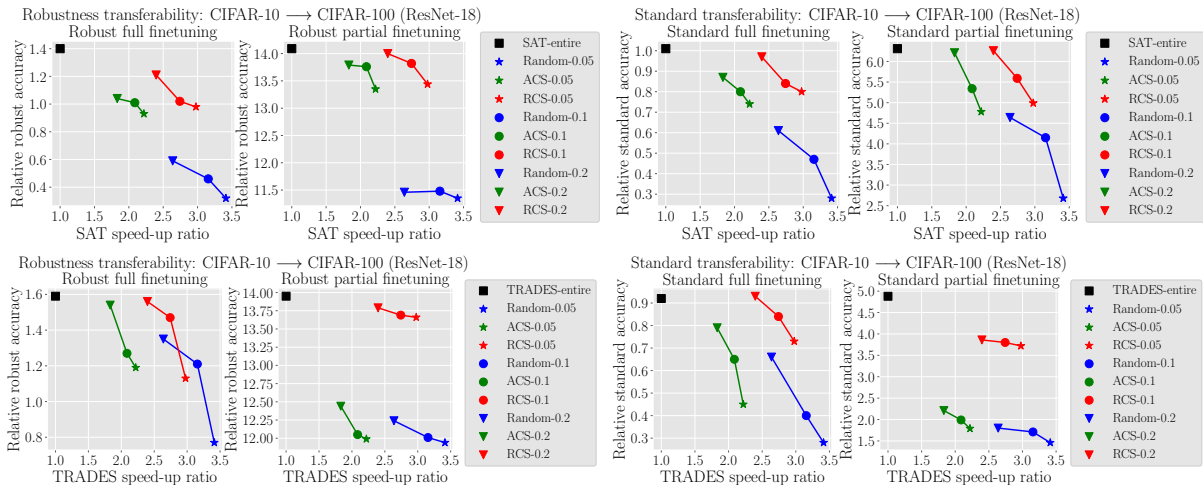


Figure 10: Transferability from CIFAR-10 to CIFAR-100 of SAT (upper panels) and TRADES (lower panels) pre-trained ResNet-18. “entire” denotes supervised AT on the entire training set of CIFAR-10. The number after the dash line denotes the subset fraction  $k \in \{0.1, 0.2, 0.3\}$ .

WRN-28-10 with different subset fractions  $k \in \{0.05, 0.1, 0.2\}$  and then conducted robust finetuning on CIFAR-10 and CIFAR-100.

To evaluate the robustness transferability of pre-trained WRN-28-10 models via SAT, we adversarially trained the pre-trained models on CIFAR-10 and CIFAR-100 for 30 epochs using SGD with the initial learning rate 0.01 and a cosine annealing scheduler. The learning objective of robust finetuning exactly follows  $\mathcal{L}_{\text{Robust}}(\cdot)$  shown in Section 2.2. The results are shown in the upper panels of Figure 4.

Following Salman et al. (2020), we pre-trained ResNet-50 models on ImageNet-1K of  $224 \times 224$  resolution using SAT (Madry et al., 2018). The model was trained using SGD with 0.9 momentum for 90 epochs with an initial learning rate 0.1 divided by 10 at epoch 30 and 60. For PGD configurations during SAT, we set  $\beta = 256$ ,  $T_{\text{SAT}} = 3$ ,  $\epsilon_{\text{SAT}} = 4/255$ ,  $\rho_{\text{SAT}} = \frac{3\epsilon_{\text{SAT}}}{T_{\text{SAT}}}$ . We set  $T_{\text{RCS}} = 1$  during RCS. We took  $\omega = 10$  epochs for warmup, and then CS was conducted every  $\lambda = 10$  epochs. We adversarially pre-trained ResNet-50 with different subset fractions  $k \in \{0.05, 0.1, 0.2\}$  and then conducted standard finetuning on downstream tasks i.e., CIFAR-10 and CIFAR-100.

To evaluate the standard transferability of pre-trained ResNet-50 via SAT on ImageNet-1K of  $224 \times 224$  resolution, we standardly trained the pre-trained models on downstream tasks (i.e., CIFAR-10 and CIFAR-100) for 150 epochs using SGD. We set the initial learning rate 0.001 for standard full finetuning and 0.01 for standard partial finetuning. The learning rate is divided by 10 at epoch 50 and 100. Here, we use the same data augmentation as Salman et al. (2020) to resize the images of CIFAR-10 and CIFAR-100 to  $224 \times 224$ . The results are shown in the lower panels of Figure 4.